学 位 論 文

Establishment of a Novel Method for Differentiating into Dopaminergic Neurons Using Charged Hydrogels

(基質荷電を用いたドパミン作動性神経細胞への新規分化法及び治療法の確立)

2025 年 3 月

北 海 道 大 学

Fan Bin

范 彬

学 位 論 文

Establishment of a Novel Method for Differentiating into Dopaminergic Neurons Using Charged Hydrogels

(基質荷電を用いたドパミン作動性神経細胞への新規分化法及び治療法の確立)

2025 年 3 月

北 海 道 大 学

Fan Bin

范 彬

Table of Contents

List of Publications and Presentations

List of Publications

(1) 題目 Title：Establishment of a Novel Method for Differentiating into Dopaminergic Neurons Using Charged Hydrogels

(2) 著者名 Name of the author：Bin Fan, *Satoshi Tanikawa, Lei Wang, Takayuki Nonoyama, Yashitaka Oda, Zenichi Tanei, Jiang Ping Gong, Masumi Tsuda, *Shinya Tanaka

(3) 掲載英文学術雑誌 Name of English publication：Biochemical and Biophysical Research Communications (BBRC)

(4) 掲載年月 Date of publication: Accepted

(5) Impact Factor：2.5

Summary

Background and Purpose

Parkinson's disease (PD) is a long-term neurodegenerative disease of mainly the central nervous system that affects both the motor system and non-motor systems. The classic symptoms of PD result from selective degeneration of dopaminergic (DA) neurons in the substantia nigra pars compacta (SNpc).

For now, cell replacement therapy is considered as a suitable treatment to replace the lost neurons. And differentiation of human induced pluripotent stem cells (iPS cells) to DA neurons has been suggested to provide such a model system.

The aim of this study was to develop the protocol based on substrate to cultivate the cells. I developed the new substrate using an electrically charged hydrogel so that allowed to generate very consistent numbers of matured DA neurons from human iPS cells lines which could generate dopamine.

Materials and Methods

The charged hydrogel was made by cationic monomer, 3-(acryloylaminopropy)-trimethylammonium chloride (APTMA), anionic monomer, 2-acrylamido-2-methylpropane sulfonic acid (NaAMPS), and dimethylacrylamide (DMA) was employed as a neutral monomer.

The iPS cells were plated on PS dish (polystyrene) and hydrogels in stem cell induction medium AK02N. From day 0 to day 12, DA neural induction was performed using Glasgow's MEM (GMEM) supplemented with 8% KnockOut Serum Replacement (KSR), 0.1 mM MEM nonessential amino acids, 100 mmol/L sodium pyruvate, and 0.1 mM 2-mercaptoethanol. Then 100um LDN193189, 500um A-83-01, 1mM Purmorphamin , 100ug/ml fibroblast growth factor 8 (FGF8) and 3mM CHIR99021 were added in different time pried to induce DA progenitor cells (DAPs). After day 12, change the medium to the neural differentiation medium containing Neurobasal medium supplemented with B27 supplement, 2 mM L-glutamine, 10 ng/ml glial cell line-derived neurotrophic factor (GDNF), 200 mM ascorbic acid, 20 ng/ml brain-derived neurotrophic factor (BDNF), and 400 mM bucladesine (dbcAMP) were added in this time. Then cultured with the neural differentiation medium until day 28.

I have checked the expression levels of mRNA and protein which are involved in DA differentiation by using RT-PCR and western blot. The expression level of L-dopa and dopamine was checked by ELISA. The pathways expression was checked by RNA sequence, A Gene Ontology (GO) enrichment test and Kyoto Encyclopedia of Genes and Genomes (KEGG) pathway analysis.

Statistical analysis: Graphical data are presented as means and standard deviation. Student's t-test was used for comparisons, with $P < 0.05$ considered significant.

Results

1. The physical properties of the charged hydrogel

A series of synthetic hydrogels that focus on having the concentration of cationic and anionic charge was developed in my thesis. They were constructed in different ratios.

The zeta potential charge analysis shows that the whole gels possessed negative charge, and was from -41 mV to -6mV. And the modulus was from 25 kPa to 80 kPa.

2. The charged hydrogels efficiently induced DA neurons

First, I tested cell culture on multiple hydrogels with varying ratios of cationic, anionic, or neutral monomers. On most hydrogels, cells either failed to adhere and proliferate, forming spheres on the gel surface or underwent cell death. However, on C1A9 and C2A8 hydrogels, cell attachment and proliferation were observed.

Next, I compared mRNA and protein expression of markers specific to DA differentiation. On the C1A9 and C2A8 hydrogels, tyrosine hydroxylase *(TH)* mRNA expression was significantly higher compared to the PS control. A concomitant decrease in the mRNA levels of stemness-related marker genes octamer-binding transcription factor 4*(Oct 3/4)* and homeobox protein *(Nanog*) was observed. Compared to the PS dish group, *Oct3/4* and *Nanog* levels decreased by 50% and 55%, respectively. Additionally, neural differentiation markers polysialylated neuronal cell adhesion molecule *(PSA-NCAM)* and microtubule-associated protein 2 *(MAP2)* showed increased expression in the group differentiated on the gel. Markers for DA neuron's differentiation, such as *TH*, aromatic l-amino acid decarboxylase (*AADC)* and dopamine transporter *(DAT)*, as well as midbrain differentiation markers like atrial natriuretic peptide-converting enzyme (*CORIN)*, nuclear receptor related 1 *(NURR1)* and forkhead box A2 *(FOXA2)* showed increased expression significantly in the gel samples. In western blot analysis, TH was detected at day 12 in PS dish group, while it could be observed at day 7 in gel groups. Besides, in day 28, the expression level of TH and AADC were increased in both gels. Next, I performed immunofluorescence analysis for TH on cells that had been cultured and induced to differentiate. The TH-positive cells in gel group were higher than PS group. These results indicate that DA differentiation of iPS cells was promoted on charged gels.

3. DA cells differentiated on charged gels show an early enhancement in dopamine production capacity.

Next, I examined the functionality of differentiated DA cells by assessing their L-dopa and dopamine production capabilities through both *in vitro* and *in vivo* experiments. The concentrations of L-dopa and dopamine in the culture medium were measured using ELISA. Specifically, the expression level of L-dopa and dopamine in gel group was higher than the PS group. *In vivo* assay, the result was similar.

In RNA sequence analysis, I calculated the fold change by dividing the gene expression of each differentiated sample by that of the undifferentiated control. On the other hand, genes with more than a two-fold decrease. These results indicate that the stem cell characteristics of hiPS_day0 were lost during differentiation, and neuronal differentiation was strongly promoted in all three groups.

Next, a pre-ranked gene set enrichment analysis (GSEA) analysis was conducted to explore differences in gene expression profiles among the differentiated samples. Pathways significantly activated in C1A9 and C2A8 included many related to neuronal differentiation, particularly pathways associated with DA neurons, such as catecholamine secretion and dopamine transport. Additionally, the database for annotation, visualization and integrated discovery (DAVID) analysis using the gene list with more than a two-fold increase which were visualized as an interactive graph using REduce + VIsualize Gene Ontology (REVIGO). These results suggest that iPS cells induced to differentiate on hydrogels show more advanced neuronal differentiation and enhanced differentiation towards DA neurons. Finally, qPCR was performed to support these results.

Discussion

The most significant differences between the hydrogel and PS dish are surface charge and stiffness. The hydrogel is considerably softer than the PS dish. In this thesis, I observed an early promotion of neural differentiation on the hydrogel compared to the PS dish, suggesting that substrate stiffness may have influenced this outcome. Additionally, surface charge may provide distinct stimuli to adherent cells by affecting protein adsorption from the culture medium or proteins secreted by the cells, or by directly influencing membrane potential. In this thesis, I developed the hydrogel system to investigate the concentration-dependent effect of cationic and anionic charge on the behavior of iPS cells in 2D cultures. The stiffness and charge promoted the differentiation of iPS cells into DA neurons, furthermore, GSEA analysis revealed activation of various pathways, in addition to promoting DA neuron differentiation.

Conclusion

In summary, I found that the C1A9 and C2A8 gels could induce the differentiation of DA neurons more efficiency, and this phenomenon may be referred to as hydrogel-activated promotion. One limitation of this study is that the essential chemical and/or physical factor(s) of the C1A9 and C2A8 gels were not directly described and 100% precisely controlled, so further study is required.

List of Abbreviations

AA: Ascorbic Acid
AADC: Aromatic L-amino acid decarboxylase
APTMA: 3-(acryloylaminopropy)-trimethylammonium chloride
APS: 0.4% (v/v) ammonium persulfate
BBB: Blood-brain barrier
BDNF: Brain-derived neurotrophic factor
CORIN: Atrial natriuretic peptide-converting enzyme
CHRNB2: Neuronal acetylcholine receptor subunit beta-2
CNR1: Cannabinoid receptor 1
CACNB3: Voltage-dependent L-type calcium channel subunit beta-3
CGA: Chromogranin-A
DA neurons: Dopaminergic neuron
DAPs: Dopaminergic progenitors
DAT: Dopamine transporter
DMA: Dimethylacrylamide
DRD1: Dopamine receptor D1
DRD2: Dopamine receptor D2
dbcAMP: Bucladesine
FOXA2: Fork head box protein A2
FGF8: Fibroblast growth factor 8
GABBR1: Gamma-aminobutyric acid B receptor 1
GAPDH: Glyceraldehyde 3-phosphate dehydrogenase
GDNF: Glial cell line-derived neurotrophic factor
IPS cells: Induced pluripotent stem cells
L-dopa: Levodopa, L-3,4-dihydroxyphenylalanine
Lmx1B: LIM homeobox transcription factor 1-beta
MAO-B: Monoamine oxidase B
MPTP: 1-methyl-4-phenyl-1,2,3,6-tetrahydropyridine
MPP^+: Hydrophilic metabolite 1-methyl-4-phenyl-pyridinium
mDA: Midbrain dopaminergic neurons
mRNA: Messenger ribonucleic acid
NaAMPS: 2-acrylamido-2-methylpropane sulfonic acid, sodium salt
NURR1: Nuclear receptor related 1

PD: Parkinson's disease

PBS: Phosphate-buffered saline

PS: Polystyrene

PCR: Polymerase chain reaction

PRKCB: Protein kinase C beta type

RNA: Ribonucleic acid

SYT3/5/6: Synaptotagmin-3/5/6

SNCG: Gamma-synuclein

TH: Tyrosine hydroxylase

TEMED: N, N, N', N'-tetramethylethylenediamine

UV: Ultraviolet

6-OHDA: Oxidopamine, 6-hydroxydopamine

Introduction

1. Parkinson's disease

Parkinson's disease (PD) is a long-term neurodegenerative disease of mainly the central nervous system that affects both the motor system and non-motor systems. Usual symptom is known as parkinsonism, including resting tremor, bradykinesia (slowness of movement), rigidity, and other symptoms that decrease quality of life, ultimately leading to significant disability via the inability to control motor function (Davie CA, 2008; Harris MK et al, 2009). The classic symptoms of PD result from selective degeneration of dopaminergic (DA) neurons in substantia nigra pars compacta (SNpc). Additionally, there is no cure for PD, treatment mainly aims to mitigate the symptoms. Initial treatment typically includes L-dopa, monoamine oxidase-B (MAO-B) inhibitors, or dopamine receptor agonists. Patients could be improved significantly after the treatment. However, the benefits of the drugs tend to diminish or erratic over time. Moreover, the pathophysiological mechanisms causing PD are poorly understood, and thus experimental systems allowing to study DA neuron dysfunction are needed.

2. The cell replacement therapy for PD

For now, cell replacement therapy is considered as a suitable treatment to replace the lost neurons (Doi D et al, 2014). In addition, in order to move on and decipher the molecular pathology that leads to DA neurodegeneration, human cell-based model systems are essential and differentiation of iPS cells to DA neurons has been suggested to provide such a model system (Jiang SZ et al, 2024).

3. DA neurons generated from iPS cells

DA neurons could be generated from human induced pluripotent stem (iPS) cells using various published protocols (Chambers SM et al, 2009; Friling S et al, 2012; Xi J et al, 2012). Among them, Doi et al (Doi D et al, 2014) has been successfully exploited, showing that significant improvement of the motor behavior, without tumor formation. Therefore, it is considered as a favorable strategy in terms of scalability, safety, and efficiency and may be advantageous for clinical application. And recently, the pre-clinical study, which evaluated the safety and efficacy of dopaminergic progenitor cells (DAPs) derived from a clinical-grade iPS cells line, has been confirmed that the characteristics of DAPs by *in vitro* analyses (Doi D et al, 2020). However, there are still have challenges that DA neurons may require an extended duration for their complete maturation into functional DA neurons. Therefore, the aim

of my experiments is improving the differentiation of DA neurons with a novel method.

On the other hand, there are several breakthroughs in the differentiation of DA neurons. Razan Sheta et al (Sheta R et al, 2022) found that combines neurogenin-2 programming with iPS cells could promote the mature and functional induced DA neurons, with minimum contamination by other brain cell types. Yi Han Ng et al (Ng YH et al, 2021) reported that the proneural factor *(Ascl1)* in combination with mesencephalic factors LIM homeobox transcription factor 1 alpha *(Lmx1a)* and nuclear receptor related 1 (*NURR1)* could induce the peripheral DA neurons. Besides, the additional midbrain transcription factors engrailed homeobox 1*(En1)*, forkhead box A2 (*FOXA2)*, and pituitary homeobox 3 *(Pitx3)* resulted in facile and robust generation of functional DA neurons of midbrain character. Moreover, Yingchao Xue et al (Xue Y et al, 2019) used synthetic mRNAs coding two proneural transcriptional factors (TFs): atonal BHLH transcription factor 1 (*Atoh1)* and neurogenin 2 *(Ngn2*) to differentiate induced iPS cells into midbrain DA neurons. And mRNAs coding *Atoh1* and *Ngn2* with defined phosphosite modifications led to higher and more stable protein expression, and induced more efficient neuron conversion, as compared to mRNAs coding wild-type proteins. Sameehan Mahajani et al (Mahajani S et al, 2019) developed a protocol based on human alpha-globin gene (HBA) promoter-driven transient expression of transcription factors by means of adeno-associated viral vectors, that allowed to generate very consistent numbers of DA neurons. Although each method has its merit, there is still a problem. That is the cell requires an extended duration for their complete maturation. Besides, the cells cannot generate large amount of L-dopa and dopamine even cannot generate them. However, in my method, the ability of expressing L-dopa and dopamine, the bio-function of DA neurons was largely improved. In addition, the time of differentiation was shortened compared to these protocols.

4. Charged hydrogel

Hydrogels are promising soft materials as tissue engineering scaffolds, stretchable sensors, and soft robotics. It is a promising candidate material for the construction of soft electronics and biomedical devices due to its mechanical flexibility, structural permeability and biocompatibility. Jinchang Zhu et al (Zhu J et al, 2024) found that multi-channel print nozzles are developed to allow on-demand mixing of highly viscoelastic bio-inks without significantly impairing cell viability. Yejin Jo et al (Yejin Jo et al, 2024) reported that universal hydrogel electronic materials could

provide a reliable platform for integrating soft electronic applications. What is more, Feng Xu et al (Xu F et al, 2024) demonstrated that hydrogel scaffolds with tissue-mimicking patterns were printed for cultivating cardiac tissue and vascular scaffolds, which can effectively support tissue growth and induce tissue morphologies. In a word, different kinds of hydrogel could promote the differentiation of cells. And it is known that surface charge and wettability of artificial substrate could contribute to cell adhesion on scaffold, and surface charge of the substrates may directly affect adhesion of cellular membrane proteins. Recent research about electrically hydrogels has begun to create new possibilities for implantable bioelectrodes (Liu Y et al, 2019; Yuk H et al, 2020), tissue engineering platforms (Park J et al, 2020), solar-powered water treatment (Zhou X et al, 2019; Li L et al, 2020), and other advanced technologies (Mo F et al, 2021).

Recently, there has been a discovery of innovative hydrogels that prioritize the electrical charge of the substratum in the context of cellular adhesion, that is electrical charged hydrogels could effectively reprogram cells by changing their adhesion and cellular membrane proteins (Wang Y et al, 2019; Martin Frauenlob et al, 2019; Suzuka J et al, 2022). And it was reported that neuronal tissue engineering was performed by using electrically charged hydrogels (Mu Q et al, 2022; Tanikawa S et al, 2023). Namely, the regeneration of neuronal tissue could be achieved through this hydrogel.

In this thesis, two kinds of electrically charged hydrogels were found, which composed of cationic and anionic monomers in 1:9 and 2:8 ratio, were suitable for the attachment, growth, and differentiation of DA neurons. Furthermore, DA neurons differentiated in these gels led to effective survival, migration, and differentiation.

5. The animal model of PD

On the other hand, in order to testify my assume, the hydrogels-induced DA neurons should be injected to the PD animal models. And there are several methods about how to establish PD animal models and these models are essential to understand the detailed pathophysiological mechanisms of PD, even to develop novel therapeutics including pharmaceutical treatments. Although it is difficult to establish such a model satisfying all of these validities, various animals as PD models have been used to date: nonhuman primates from big monkeys, such as baboons (Kishima H et al, 2004) and macaques (Saiki H et al, 2010) to small ones, common marmosets (Choudhury ME et al, 2010), rodents especially rats and mice, rabbits (Ghribi O et al, 2003), dogs (Choi CB et al, 2011), cats (Schneider JS and Rothblat DS, 1991), frogs

(Barbeau A et al, 1985) and nonvertebrate drosophila (Park J et al, 2005) and nematode (Braungart E et al, 2004). Among them, nonhuman primates are especially valuable because of their genetic, anatomical, and functional similarities to humans, although there are some difficulties regarding availability, habitation, handling, and experimental techniques. The most frequently used animals are rats and mice as they are readily available and easy to handle.

6. **MPTP**

For now, the typical neurotoxins and chemicals for PD models including Neurotoxin 1-Methyl-4-Phenyl-1,2,3,6-Tetrahydropyridine (MPTP), 6-hydroxydopamine (6-OHDA), pesticides (such as rotenone, paraquat, and maneb) and some other chemicals. Among them, MPTP and 6-OHDA are the most commonly used. However, because of low permeability to blood–brain barrier (BBB), the 6-OHDA must be applied directly into specific region of brain (typically in substantia nigra, medial forebrain bundle, or striatum) using stereotactic apparatus. For this reason, rats are most frequently used and less applied in nonhuman primates (Betarbet R et al, 2002). So, in my research, MPTP was chosen to be used in the establishment of mice PD model.

MPTP is an organic compound. It is classified as a tetrahydropyridine. And because it is a highly lipophilic molecule which could easily cross BBB and be converted into the hydrophilic metabolite 1-methyl-4-phenyl-pyridinium (MPP^+) by MAO-B expressed in astrocytes. MPP^+ is selectively incorporated into DA neurons via dopamine transporter (DAT), and is taken up into mitochondria, inhibiting complex I of the respiratory electron transfer chain. This leads to impairment of ATP production, elevated intracellular $Ca2^+$ levels, and generation of reactive oxygen species/reactive nitrogen species (ROS/RNS), eliciting apoptotic cell death of the DA neurons. Thus, MPP^+ is primarily a mitochondrial toxin to specifically disrupt the respiratory system of DA neurons (Yokoyama H et al, 2011). MPP^+ also triggers inflammatory reactions starting from activation and proliferation of astrocytes and microglia (Yokoyama H et al, 2011). It facilitates synthesis and secretion of inflammation-related molecules including cytokines, such as tumor necrosis factor (TNF-α), interleukin 1β (IL-1β) and interleukin 6(IL-6), chemokines, and prostagrandines. In microglia, upregulation of inducible NO synthase (iNOS) also occurs, resulting in increase and release of NO, which attacks neurons with generating toxic ROS and RNS. These events are well consistent with what happened in the brain of PD patients mentioned earlier.

In the establishment of PD animal models, mice are more favorably used than other kinds of animals because the latter show a relatively high peripheral MAO activity (Kalaria RN et al, 1987) causing conversion of MPTP to MPP^+ before crossing BBB, failing to enter brain.

7. Aim of this thesis

The aim of this thesis was to develop the protocol based on using an electrically charged hydrogel so that allowed to generate very consistent numbers of matured DA neurons from human iPS cells lines which could generate dopamine. It is a development of a method to induce DA activity more efficiently than before. Moreover, the pathophysiological mechanisms causing PD are poorly understood, and thus experimental systems allowing to study DA neuron dysfunction are needed. In conclusion, it was found that the C1A9 and C2A8 gels could induce the differentiation of DA neurons more efficiency, and this phenomenon may be referred to as hydrogel-activated promotion. Suggesting a novel method for the completely treatment of PD. At the same time, it also provides a new idea for the transformation of iPS cells into other kind of cells.

Methods

1. Preparation of hydrogels with various charges.

Hydrogel sheets with a thickness of 1 mm were synthesized by using two parallel glass plates. To synthesize the differentially charged hydrogel, various combinations of a cationic monomer, 3-(acryloylaminopropy)-trimethylammonium chloride (APTMA) (Tokyo Chemical Industry Co., Ltd., Tokyo, Japan), and an anionic monomer, 2-acrylamido-2-methylpropane sulfonic acid (NaAMPS) (Sigma-Aldrich, St. Louis, MO, USA) were used. Dimethylacrylamide (DMA) (Sigma-Aldrich) was employed as a neutral monomer.

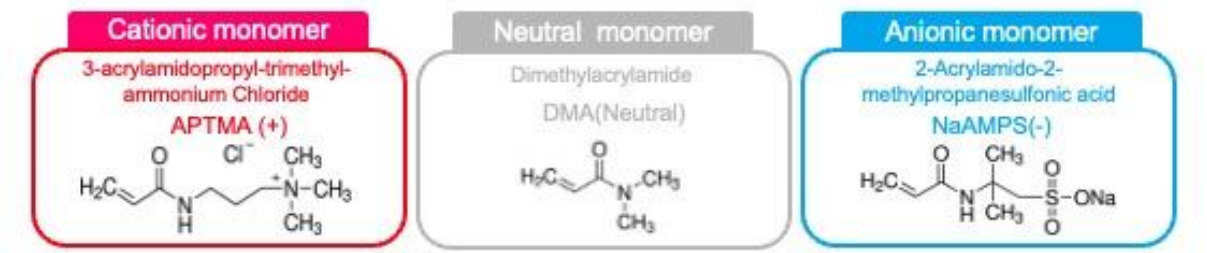

Several differentially charged hydrogels were constructed. The ratios of cationic (C) and anionic (A) monomers of 0:10, 1:9, 2:8, 3:7, and 4:6, which were designated as C0A10, C1A9, C2A8, C3A7, and C4A6 gels; the ratios of C and neutral (N) monomers of 10:0, 2:8, 3:7 as C10N0, C2N8, C3N7; and the ratios of A and N

monomers of 2:8 as A2N8 respectively. Polymerization of 1 M monomer was performed with 4 mol% N, N'-meth-ylene-bis-acrylamide (Sigma-Aldrich) as a crosslinker with 0.1% (v/v) N, N, N', N'-tetramethylethylenediamine (TEMED) (Wako Pure Chemical Ind., Ltd., Japan) and 0.4% (v/v) ammonium persulfate (APS) (Wako) at room temperature overnight.

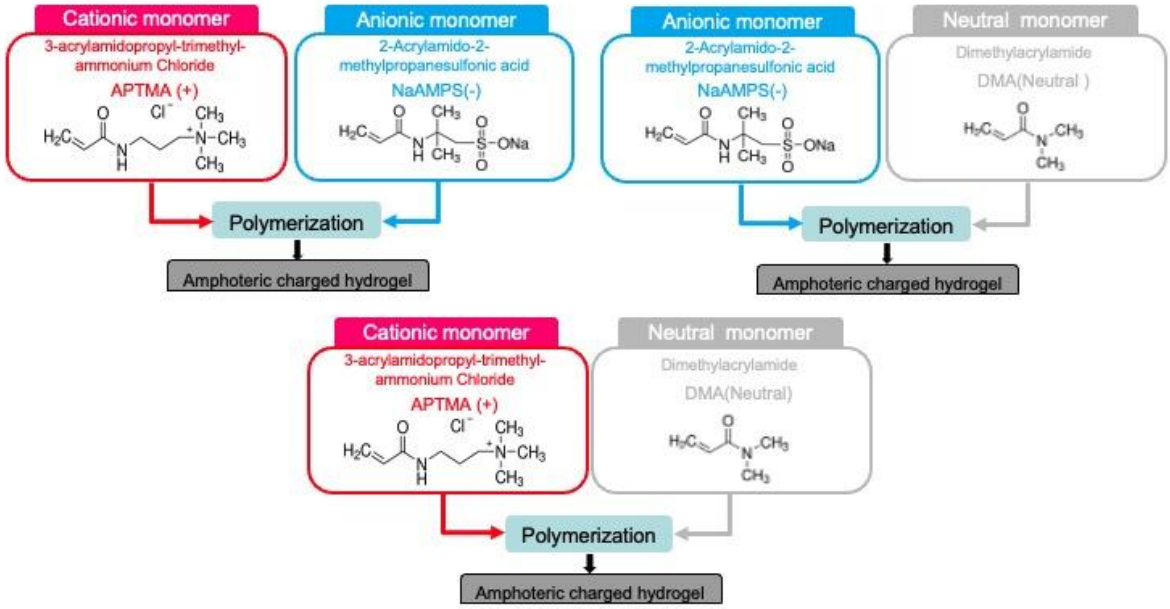

Alternatively, UV irradiation was used for polymerization. Polymerized hydrogels were immersed in a large amount of phosphate-buffered saline (PBS) to remove residual unpolymerized chemicals for 1 week, and the PBS was refreshed every day. Subsequently, gel disks were punched out of the gel sheet with a hole punch and sterilized in an autoclave at 120 °C for 20 min without significant decomposition. The gel disks were then placed on PS tissue culture dishes and equilibrated in cell culture medium overnight.

Measurement of the mechanical and physical properties of hydrogels

(i) Measurement of Young's modulus

Surface moduli of gel samples were evaluated by microindentation. The tip geometry of the stainless indenter was a 1.0 mm radius hemisphere. I measured the force-displacement curves of the gel surfaces at 1 mm/min test speed on the mechanical tester (Universal testing machine AGX-V, Shimadzu, Japan). According to the Hertz model (C.T. McKee et al, 2011) of contact between hemisphere indenter and planar sample, the relation of force (F) and displacement (d) is described as:

$$d = \left[\frac{3}{4}\left(\frac{1-\nu_s{}^2}{E_s} + \frac{1-\nu_i{}^2}{E_i}\right)\right]^{2/3} \cdot F^{2/3} \cdot R^{-1/3}$$

where $E_{s\ (i)}$, $v_{s\ (i)}$, and R are sample (indenter) modulus, sample (indenter) Poisson's ratio, and radius of indenter tip, respectively. When $E_s << E_i$, $\overline{1-{\nu_i}^2/E_i}$ is regarded as zero. Therefore, the above equation can transform to:

$$F^{2/3} = \left[\frac{3}{4}\left(\frac{1-{\nu_s}^2}{E_s}\right)\right]^{-2/3} \cdot R^{1/3} \cdot d$$

F

To calculate E_s, sample Poisson's ratio v_s was set at 0.5 because of incompressibility and isotropy of the gel samples.

(ii) Zeta potential measurement

The surface electric charge of the hydrogel was measured as the zeta potential by using a Zeta-potential & particle size analyzer (ELSZneo, Otsuka Electronics, Osaka, Japan) For the detection of potential, a standard particle suspension (500–600 nm in diameter; Otsuka Electronics) consisting of a PS-latex core with a hydroxypropyl cellulose shell was diluted 300 times with a 10 mM sodium chloride (NaCl) aqueous solution. A specimen sheet was placed on a quartz block cell with a liquid-flow passage, and the standard particle-dispersed solution was used to fill the passage. The zeta potential was evaluated by laser-Doppler electrophoretic light scattering (ELS) (n = 3).

2. Preparation and culture of iPS cells

The HPS0063 201B7 iPS cells lines applied in this study was brought from the Center for iPS cell Research and Application (CiRA) (Kyoto University, Kyoto, Japan). iPS cells were plated on PS dish and hydrogels coated with iMatrix-511 silk (TaKaRa, T311-892021, Kyoto, Japan) and cultured for 5 days in stem cell induction medium StemFit® AK02N (AK02N, AJINOMOTO, Tokyo, Japan) after the density of 2×10^4, the iPS cells were used for experiments.

The protocol of DA neural induction from human iPS cells. DA neural induction was performed using pharmacological compounds as published (Doi D et al, 2014). When the iPS cells reached a confluent state, and StemFit® AK02N were changed to the differentiation media containing Glasgow's MEM (GMEM) (Wako, 078-05525) supplemented with 8% KnockOut Serum Replacement (KSR) (Thermo Fisher Scientific, 10828-028, Waltham, MA, USA), 0.1 mM MEM nonessential amino acids (Invitrogen, 06344-56, Waltham, MA, USA), 100 mmol/L sodium pyruvate (Sigma-Aldrich, 06977-34), and 0.1 mM 2-mercaptoethanol (Sigma-Aldrich, M6250). I added LDN193189 (STEMGENT, 04-0074-02, Tokyo, Japan) and A-83-01 (Wako, 039-24111) to efficiently induce neuronal differentiation. Purmorphamine (Sigma-Aldrich, 483367-10-8) and fibroblast growth factor 8 (FGF8) (Wako,

063-04371) were added from day 1 to day 7, and CHIR99021 (Wako, 252917-06-9) from day 3 to day 12 to induce the DAPs. In the published protocol (Doi D et al, 2014), the DAPs need to be selected atrial natriuretic peptide-converting enzyme *(CORIN)*-positive cells in cell sorting by the fluorescence-activated cell sorting (FACS) on 12 days, I also attempted sorting using CORIN, however, due to potential issues with the antibody or technical challenges (if the DAPs were collected from hydrogels to have the cell sorting, they cannot adhere to the hydrogels again), I was unable to establish a reliable protocol. In the further research, there is still room for improvement.

After day 12, change the medium to the neural differentiation medium containing Neurobasal medium supplemented with B27 (Gibco, Thermo Fisher Scientific, 17504-044) supplement, 2 mM L-glutamine, 10 ng/ml, glial cell line-derived neurotrophic factor (GDNF) (Wako, 070-06261), 200 mM ascorbic acid (Sigma-Aldrich, 102605753), 20 ng/ml brain-derived neurotrophic factor (BDNF) (Wako, 020-12913), and 400 mM bucladesine (dbcAMP) (Sigma-Aldrich, 241-059-4). Thirty mM of Y-27632 (Wako, 331752-47-7) was added in the first medium to avoid apoptosis at the initial step. After that, medium was changed every 2 days. Then cultured with the neural differentiation medium until day 28.

In Doi et al (Doi et al, 2014), cells were cultured on iMatrix coated PS dishes for 12 days, followed by sorting with CORIN, and then suspended culture. The suspended culture was likely intended for transplantation purposes, and thus, few paper suggested that suspended culture is more suitable for DA neuron differentiation.

In my data, the control condition used iMatrix coated PS dishes, and at day 12 of the adhesion culture period, neural markers were already elevated in the gel condition. Therefore, the comparison at this stage is meaningful in terms of examining how the substrate stiffness or charge influences differentiation. What is more, the charged hydrogel is structured as a flat-bottom plate, so PS is much easier to set hydrogel. On the other hand, few paper reported the “best” culture conditions for the differentiation of DA neurons, namely, there is space for improvement in the future research.

3. The injection of DA neurons to the C57BL/6JJcl mice

After 28 days culture, the DA neurons were collected and purified, then injected into the subcutaneous of the C57BL/6JJcl mice (CLEA, Japan) with PBS. The amount of cell is 1×10^7 cells 1 time, then collect its serum in day 1, 3, 5, and 7.

In this thesis, all animal experiments were conducted in accordance with the guidelines of the Hokkaido University Manual for Implementing Animal

Experimentation and approved by the Institutional Animal Care and Use Committee at the Hokkaido University Graduate School of Medicine (number 22-0089).

4. Quantitative RT-PCR

Total RNA was isolated using a RNeasy Mini or Micro Kit (Qiagen, 74104, Venlo, Netherlands), and cDNA was synthesized from 2 ug of RNA using the High-Capacity cDNA Reverse SuperScript® VILO™ cDNA Synthesis Kit (Invitrogen, 11754050, Carlsbad, CA). qRT-PCR was performed using StepOnePlus™ Real-Time PCR System (Applied Biosystems, Waltham, MA) using Power SYBR Premix Ex Taq (Invitrogen) and the QuantStudio 3 System (Thermo Fisher Scientific). The data were assessed using a delta-Ct method and normalized by the *GAPDH* expression.

Table: 1 Primer sequence for PCR experiment

GAPDH

Forward: 5'-GTCTCCTCTGACTTCAACAGCG-3'

Reverse: 5'-ACCACCCTGTTGCTGTAGCCAA-3'

TH

Forward: 5'-GCTGGACAAGTGTCATCACCTG-3'

Reverse: 5'-CCTGTACTGGAAGGCGATCTCA-3'

FOXA2

Forward: 5'-GGAACACCACTACGCCTTCAAC-3'

Reverse: 5'-AGTGCATCACCTGTTCGTAGGC-3'

DAT

Forward: 5'-CCTCAACGACACTTTTGGGACC-3'

Reverse: 5'-AGTAGAGCAGCACGATGACCAG-3'

NURR1

Forward: 5'-AAACTGCCCAGTGGACAAGCGT-3'

Reverse: 5'-GCTCTTCGGTTTCGAGGGCAAA-3'

Lmx1B

Forward: 5'-GGTCCAGGTCTGGTTTCAGAAC-3'

Reverse: 5'-GTGTAGGAAGCCATCATGCCCT-3'

Brachyury

Forward: 5'- CCTTCAGCAAAGTCAAGCTCACC-3'

Reverse: 5'-TGAACTGGGTCTCAGGGAAGCA-3'

SOX17

Forward: 5'-ACGCTTTCATGGTGTGGGCTAAG-3'

Reverse: 5'- GTCAGCGCCTTCCACGACTTG-3'

DRD1

Forward: 5'-TGGTCTGTGCTGCCGTTATCAG-3'

Reverse: 5'- CAATCTCAGCCACTGCCTTCCA-3'

DRD2

Forward: 5'- CAATACGCGCTACAGCTCCAAG-3'

Reverse: 5'- GGCAATGATGCACTCGTTCTGG-3'

SYT3

Forward: 5'- TCCGAGATGCTGACACCAACGA -3'

Reverse: 5'- GCCACAGAATGTCACGATGACC -3'

SYT5

Forward: 5'- CAGACGCTGAACCCTCACTTTG -3'

Reverse: 5'- GATGGCGTCATTGCGAGAGAAG -3'

SYT6

Forward: 5'- CAGATGTCGGTCAAGGAGCACA -3'

Reverse: 5'- TGCTGGTGGAAGCTCATTGCCA -3

CHRNB2

Forward: 5'- CTCCCTTCCAAACACATCTGGC -3'

Reverse: 5'- GATGCTGCCATCATAGGAGACC -3

GABBR1

Forward: 5'- CCTGAACAAGACATCTGGAGGAG -3'

Reverse: 5'- GCTGGCATCAAACACCACATGG -3

SNCG

Forward: 5'- TGTGGTGAGCAGCGTCAACACT -3'

Reverse: 5'- TTGGATGCCACACCCTCCTGTT -3

CNR1

Forward: 5'- CTGTTCCTCACAGCCATCGACA -3'

Reverse: 5'- TGGCTATGGTCCACATCAGGCA -3

5. L-dopa and dopamine release assay

Human iPS cells-derived neural cells were differentiated on PS dish/ C1A9/ C2A8 for 28 days, then the medium was collected in day 1, day 7, day 12 and day 28. Then the concentration of L-dopa was determined by GENLISATM Human L-dopa ELISA Kit (KRISHGEN BioSystems, Mumbai, India) and dopamine research ELISA Kit (immusmol, Funakoshi Co., Ltd. Tokyo, Japan), respectively. And the serum of mice

was diluted 10 times and 20 times in L-dopa and dopamine determination, respectively.

6. Immunofluorescence staining

Cells were cultured on PS dishes and hydrogels, subsequently treated, and fixed using 4% paraformaldehyde (PFA) solution for 15 minutes in TBS, treated with 0.1% v/v Triton X-100 for 4 minutes to make the cell membrane permeable. Permeabilization was achieved by prechilled methanol treatment, followed by blocking with bovine serum albumin (1 mg/ml) for 20 min. The samples were incubated overnight at 4°C with a rabbit polyclonal antibody (anti-tyrosine hydroxylase antibody, AB152, Sigma-Aldrich, P04177) at a 1:400 dilution in PBT (PBS containing 0.1% BSA and 0.05% Triton X-100), followed by the incubation with a 1:250 dilution of Alexa 594-conjugated anti-rabbit IgG (Molecular Probes, A-11037, Oregon, USA) in PBT for 1 hour and DAPI (1 μg/ml) for 20 minutes in PBT. Samples underwent mounting and were examined using microscope (OLYMPUS IX83, Tokyo Japan). ImageJ software (National Institutes of Health, Bethesda, MD, USA) was utilized for processing cell imaging data. Nucleus fluorescence intensity was quantified as the average gray value after subtracting background intensity. Statistical analysis, including mean and p value determination, was performed based on data acquired from a minimum of 20 cells per condition.

7. Protein assay

Cells were collected from hydrogels and lysed by sonication in RIPA buffer containing 10 mM Tris pH 7.4, 0.1% sodium dodecyl sulfate (SDS), 1% deoxycholate (DOC), 10% glycerol, 1% Triton X-100 and 5 mM EDTA supplemented with protease inhibitors. Using the Protein Assay Dye Reagent Concentrate (Bio-Rad Laboratories, Hercules, CA, USA), the protein concentrations in whole-cell lysates were evaluated by Bicinchoninic Acid Assay (BCA Assay). Prepare a series of standard protein solutions with Bovine Serum Albumin (BSA) (Sigma-Aldrich, A7030) with known concentrations for generating a standard curve. Add the BCA working reagent prepared by mixing Bio-Rad Protein Assay Dye Reagent Concentrate (Bio-Rad Laboratories, 50000006) and Double Distilled Water (DDW) to each tube. Then incubate the mixture at 37°C for 5 minutes to allow the reaction to complete. After incubation, measure the absorbance at 595 nm using a spectrophotometer. The microplate reader SpectraMax ABS/ABS Plus (Molecular Devices, CA, USA) is used for high-throughput measurements. After that, generate a standard curve by plotting the absorbance values of known concentrations of protein standards. The x-axis

represents the protein concentration, while the y-axis represents the measured absorbance. Finally, calculate the protein concentration of the sample by comparing its absorbance value with the standard curve. (The standard curve does not show here)

8. Western blotting

After the assay of protein, equal protein quantities (20 μg) were then heated to 95°C for 10 minutes. which separated proteins using SDS-polyacrylamide gel, was used to transfer the proteins to PVDF membranes (Millipore, Billerica, MA, USA). Membranes were blocked in 5% non-fat dry milk in TBS-T buffer (0.1% Tween-20 in Tris-buffered saline) for 1 h at room temperature and then exposed to primary antibodies against tyrosine hydroxylase (TH) (Sigma-Aldrich, AB152, rabbit, 1:1000 dilution), aromatic l-amino acid decarboxylase (AADC) (Sigma-Aldrich, ABT264, rabbit, 1:1000 dilution) and actin (Sigma-Aldrich, SC47778, rabbit, 1:2000 dilution) at 4 °C overnight. The membranes were washed thrice with TBST (with 0.25% Triton X-100) and incubated with the respective secondary antibodies (goat anti-rabbit IgG antibody, HRP conjugate, Sigma-Aldrich, AP370P, 1:5000 dilution) for 1h at room temperature. Lab-made ECL was used and protein detection was performed with the help of X-ray detection system.

9. RNA sequence

Total RNA was extracted from iPS cells and the cells during differentiation at day 28 for both on PS dish and on C1A9 and C2A8 gels using the RNeasy Mini Kit (Qiagen, 74106). And NanoDrop One/OneC (ThermoFisher Scientific) were used to measure RNA concentration and integrity.

After the measurement, all samples were sequenced on an Illumina platform (NovaSeq 6000/Novaseq X Plus). All sequencing was performed at Rhelixa Co., Ltd. (Tokyo, Japan). Genes with an FDR < 0.05 and | log2FC|>1.1 were included in the analysis. A Gene Ontology (GO) enrichment test and Kyoto Encyclopedia of Genes and Genomes (KEGG) pathway analysis were performed using express Analyst.

Data analysis was performed using R studio version 2023.12.0+369 (R Core Team, 2023). Comparisons between samples were performed using data normalized to transcripts per million (TPM). Principal component analysis (PCA) was conducted using prcomp function, and heatmaps were generated with the pheatmap package (Kolde R, 2018). Correlation coefficients were calculated using the cor function, and the results were visualized with the ggpairs function in the GGally package (Schloerke B et al, 2022; Crowley J, 2024). The fold change between undifferentiated controls (hips day 0) and differentiated samples (hips day 28, C1A9 day 28, and C2A8

day 28) was calculated. Genes showing more than a two-fold increase were classified as upregulated, while those showing more than a two-fold decrease were classified as downregulated. The results were visualized as a Venn diagram using the ggVennDiagram function (Gao et al, 2021; Gao et al, 2024). Functional enrichment analysis was performed using the database for annotation, visualization and integrated discovery (DAVID) (Schloerke B et al, 2022) on the gene set common to all groups with more than a two-fold increase compared to the undifferentiated control. Pathway analysis was conducted using Gene Ontology (GOTERM_BP_DIRECT, GOTERM_CC_DIRECT, GOTERM_MF_DIRECT). Pathways with an adjusted p-value of less than 0.05 after Benjamini-Hochberg correction were extracted and visualized as a Treemap of Biological Processes (BP) using REduce + VIsualize Gene Ontology (REVIGO) (Supek F et al, 2011), with the results output in RStudio using the Treemap function (Tennekes M, 2023). A pre-ranked gene set enrichment analysis (GSEA) was conducted using the fold change in gene expression, directly comparing PS day 28, C1A9 day 28, and C2A8 day 28 without indirect comparison through an undifferentiated control. The gene sets used were from the ontology gene sets (C5) of Human MSigDB v2023.2. Hs (Liberzon A et al, 2015; Subramanian A et al, 2005). GSEA was performed using the fgsea package (version 1.26.0) (Korotkevich G et al, 2021), and results were ranked by Normalized Enrichment Score. Visualization and figure creation were done using the ggplot2 package (version 3.4.4) (Wickham H, 2016). Additionally, DAVID analysis was performed on gene sets with more than a two-fold increase in fold change in the direct comparison, and significant GO terms were extracted. GO term clustering and visualization showing relationships between similar GO terms were generated as an interactive graph using REVIGO, with the results output in Cytoscape (Shannon P et al, 2003).

10. MPTP-induced mice model of PD

In this research, 6-week-old male C57BL/6JJcl mice was chosen to be injected MPTP (Sigma-Aldrich, 23007-85-4). Firstly, MPTP was dissolved in water with up to 10 mg/mL. Following 20 mg/kg for 4 times with 2-h intervals as an acute model; 30 mg/kg/day for 5 days as a subacute model.

11. Statistical analysis.

Graphical data are presented as means and standard deviation. Student's t-test was used for comparisons, with $P < 0.05$ considered significant.

Results

1. The zeta potential charge and modulus analysis of the charged hydrogel

A series of synthetic hydrogels that focus on having the concentration of cationic and anionic charge was developed in my study. Cationic, anionic and neutral monomer were constructed in different ratios, The appearance of the gel is colorless and transparent after it is made (Figure 1A).

Next, is the zeta potential charge analysis shows that the whole gels possessed negative charge, and was from -6 mV to -41mV (Figure 1B) And because of different concentrations of the monomers, the modulus measured by indentation was different among these gels. It was from 25 kPa to 80 kPa (Figure 1C) The hydrogels were dialyzed in PBS in order to remove residual unpolymerized chemicals before cell seeding. The cultivation of iPS cells on non-dialyzed hydrogels was difficult because unpolymerized chemicals attribute to a low attachment followed by an increased death rate.

Figure 1

A.

B.

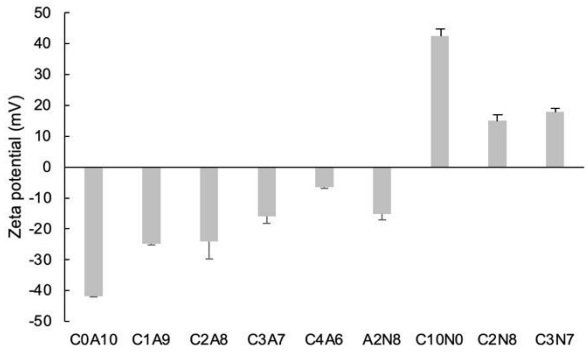

C.

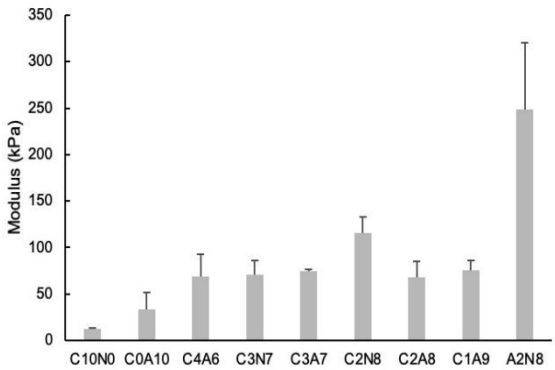

Figure 1 The analysis of physical properties of the charged hydrogels.

(A) The outlook of the gel. Scale bar = 1 mm. (B) The zeta potential analysis of the charged hydrogels such as C0A10, C1A9, C2A8, C3A7, C4A6, A2N8, C10N0, C2N8, and C3N7. (C) The compressing modulus analysis of charged hydrogel. The data represent means ± s.d. (n = 3 independent experiments). Two-sided paired t-tests were used for statistical analysis.

2. The protocol of this study

The iPS cells were plated on PS dish and hydrogels and inducted to DA neurons as mentioned previously.

After day 12, the medium and it was changed every 2 days. Then cultured with the neural differentiation medium until day 28 as described previously. (Figure 2)

Figure 2

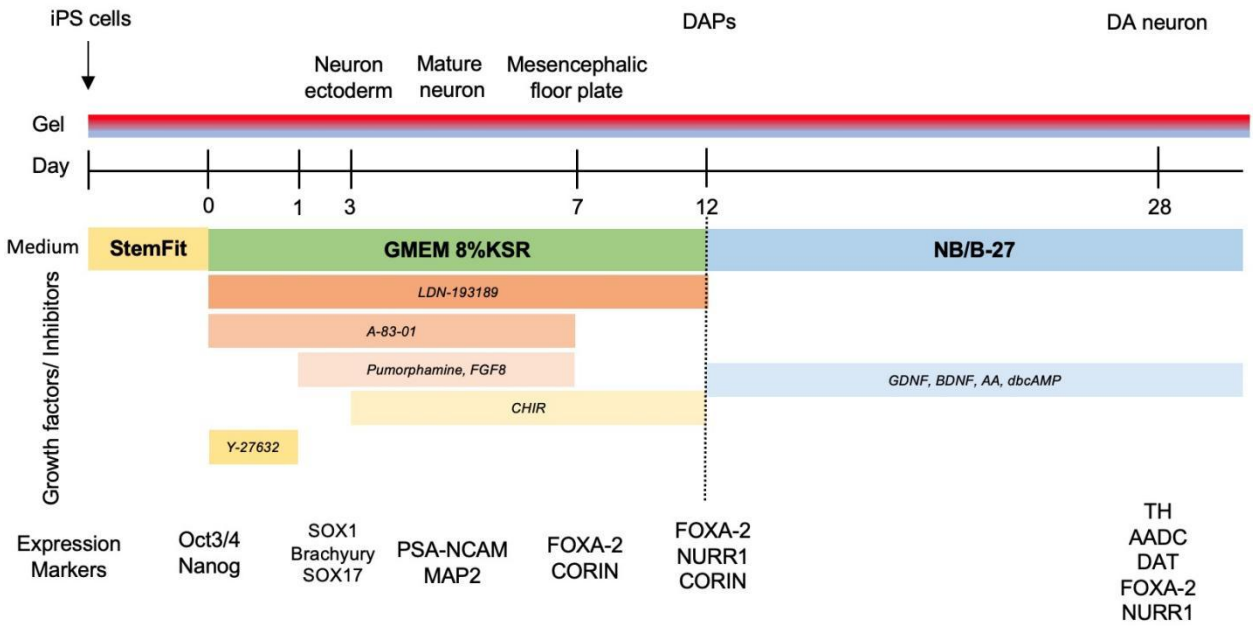

Figure 2 The protocol of this study and the different genes markers at each time.

iPS cells were seeded onto both the PS dish and each gel. After five days in culture, we changed medium for DA neuron differentiation. In different time, different markers were been checked.

3. The charged hydrogels could induce iPS cells into DA neurons

First, I investigated whether human iPS cells could attach and proliferate on charged hydrogels. I tested cell culture on multiple hydrogels with varying ratios of cationic, anionic, or neutral monomers. On most hydrogels, cells either failed to adhere and proliferate, forming spheres on the gel surface (e.g., C3A7 and C4A6; or underwent cell death (e.g., only cationic monomer, only anionic monomer, C3N7, C2N8) (Figure 3). On the other hand, on C1A9, C2A8, and A2N8 hydrogels, cell attachment and proliferation were observed. (Figure 3).

To investigate the effects of charged gels on iPS cells and DA differentiation, I differentiated human iPS cells into DA neurons on PS dish and hydrogels. The protocol basically followed the pharmacological compounds as published (Doi D et al, 2014). Firstly, I planted iPS cells were seeded onto both the PS dish and each gel. After five days in culture, I changed medium for DA neuron differentiation (Figure 2). Following seeding on C1A9, C2A8 and A2N8, cells began to aggregate and make clusters (Figure 3).

Figure 3

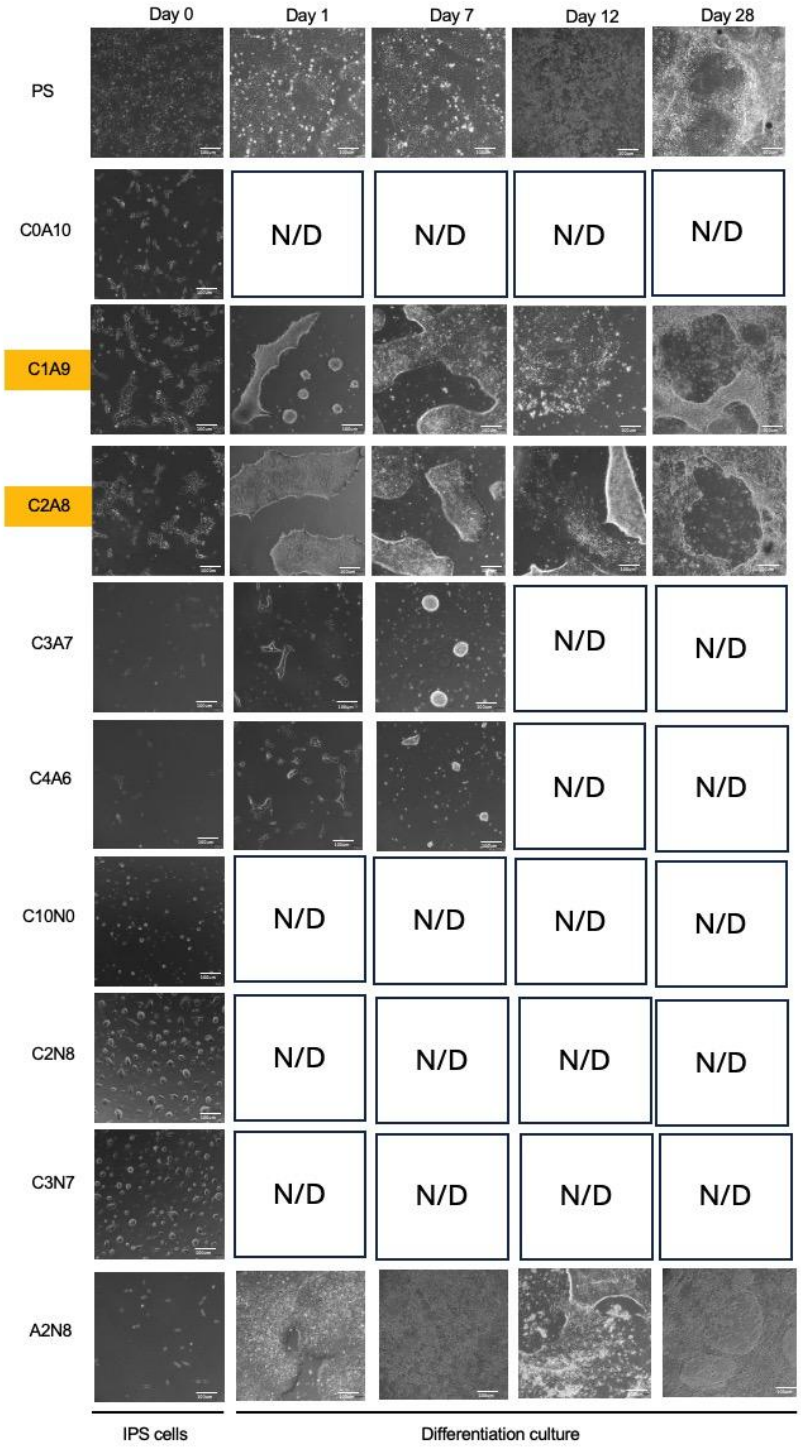

Figure 3 Analysis of the DA neurons differentiation on PS dish and charged hydrogels.

(A) The bright field images of iPS cells and differentiated DA neurons on each substrate. Scale bars = 100 μm. (B) Characteristics of iPS cells on other hydrogels. The cell could not survive on the other kinds of gels. Only on C1A9, C2A8, and A2N8 hydrogels, cell could have attachment and proliferation.

4. The charged hydrogels efficiently induced DA neurons

I next compared mRNA and protein expression of markers specific to DA differentiation. I examined the mRNA expression of *TH*, a key marker for DA neurons. On the C1A9 and C2A8 hydrogels, *TH* mRNA expression was significantly higher compared to the PS control (Figure 4A). Interestingly, cells differentiated on the A2N8 hydrogel showed a trend of lower *TH* expression relative to the control (Figure 4A). Therefore, subsequent experiments were conducted using C1A9 and C2A8. A concomitant decrease in the mRNA levels of stemness-related marker genes homeobox protein (*Nanog)* and octamer-binding transcription factor 4 *(Oct 3/4*) was observed (Figure 4B). Compared to the PS dish group, *Nanog* and *Oct3/4* levels decreased by 55% and 50%, respectively. On the other hand, in the neuroectoderm, I found that the germ layer markers SRY-box transcription Factor 1 *(SOX1),* T-box transcription factor T *(Brachyury)* and SRY-box transcription factor 17 *(SOX17)*, especially *SOX1* was obvious than *Brachyury* and *SOX17*(Figure 4C), namely, the iPS cells largely turned into ectoderm instead of mesoerm and endoderm which belongs to the neuroectoderm.

Additionally, neural differentiation markers polysialylated neuronal cell adhesion molecule *(PSA-NCAM)* and microtubule-associated protein 2 (*MAP2)* showed increased expression as early as day 7 in the group differentiated on the gel (Figure 4D). Markers for midbrain differentiation markers like *CORIN*, *NURR1* and *FOXA2* (Figure 4E), as well as DA cell differentiation, such as *DAT* and *AADC* showed increased expression significantly in the gel samples (Figure 4F). These results indicate that DA differentiation of iPS cells was promoted on charged gels.

Figure 4

A.

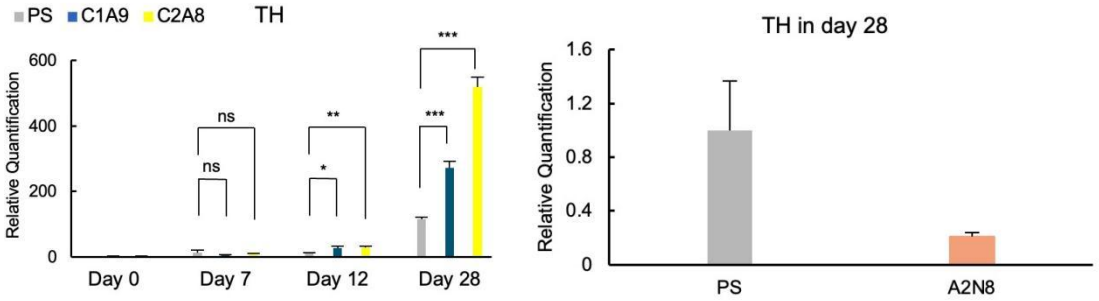

B.

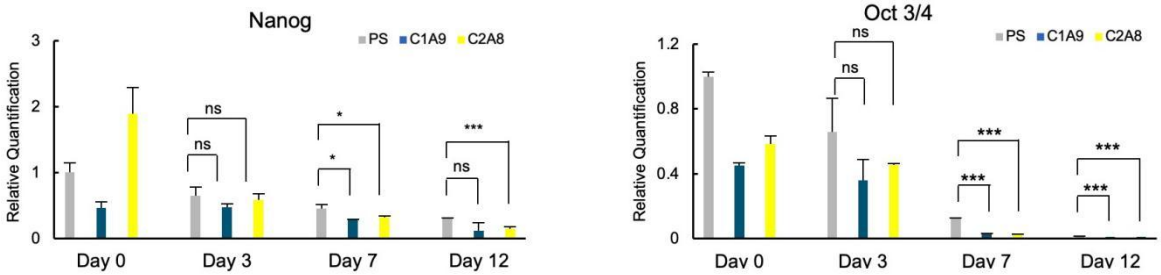

C.

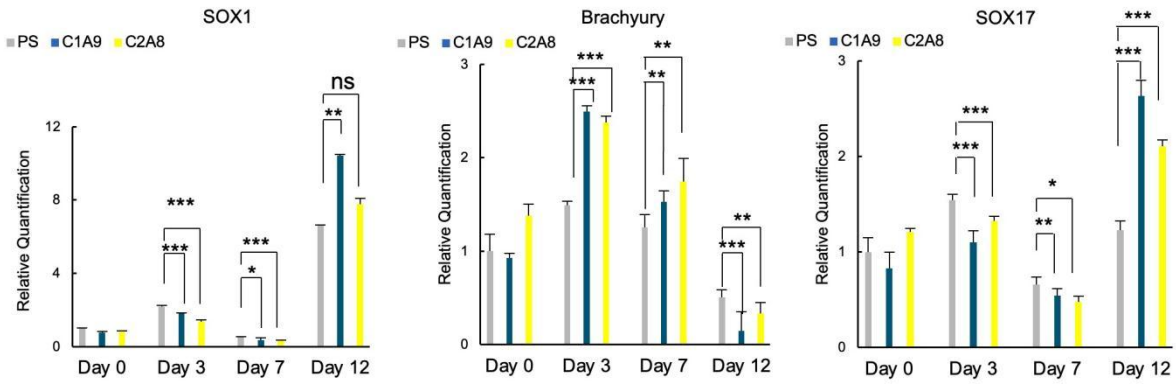

D.

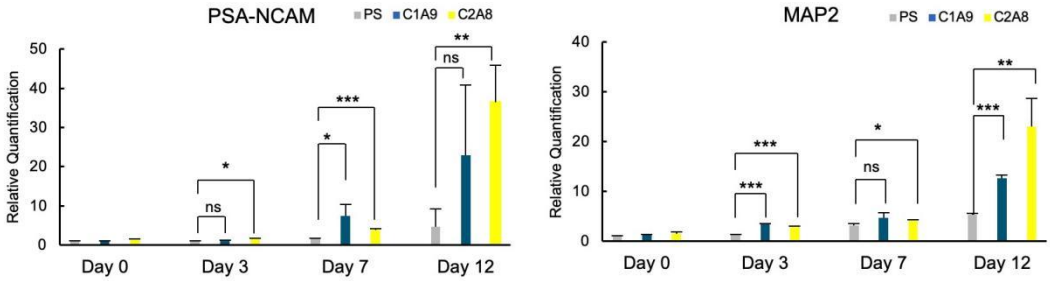

E.

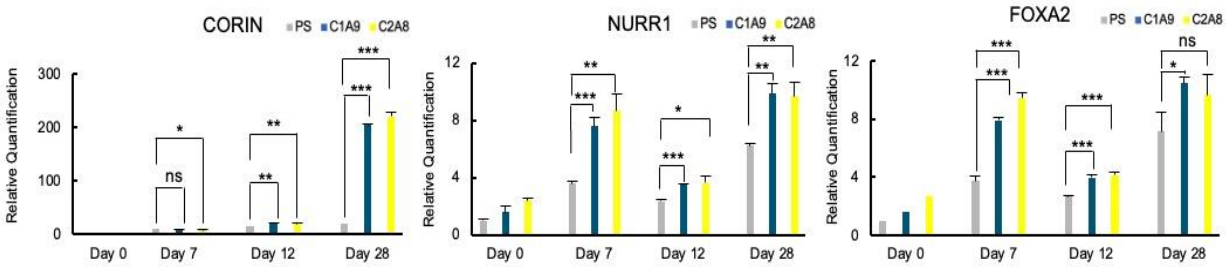

F.

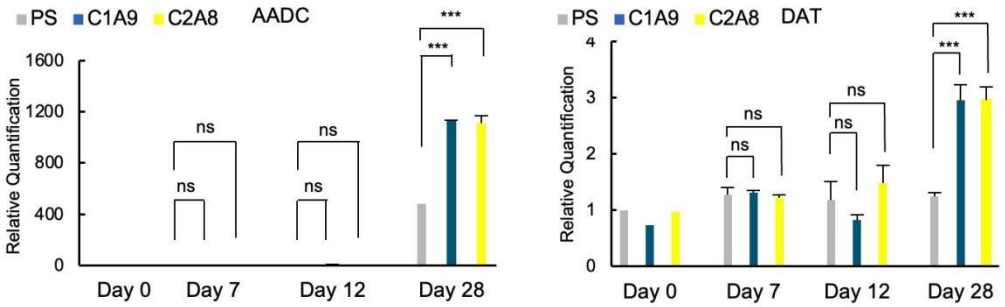

Figure 4 qPCR results for different markers.

(A) qPCR result of DA neuron markers *TH*. And iPS cells cultured on A2N8 hydrogel showed either no change or a tendency for reduced *TH* expression compared to those on PS dishes. (B)The expression levels of stemness markers *Nanog* and *Oct3/4* at each time point. (C) The expression levels of neuroectoderm markers of *SOX1, Brachyury* and *SOX17*. (D) The expression levels of neural differentiation markers *PSA-NCAM* and *MAP2*. (E)The expression levels of midbrain differentiation markers *CORIN*, *FOXA2* and *NURR1*. (F)The expression levels of DA neuron markers *AADC* and *DAT*. The data represent means ± s.d. (n = 3 independent experiments). (*P < 0.05; **P < 0.01; ***P < 0.001).

5. The expression level of proteins in charged hydrogels induced DA neurons

In western blot analysis, TH was detected at day 12 in PS dish group, while it could be observed at day 7 in gel groups (Figure 5A). Besides, in day 28, the expression level of TH and AADC were increased in both gels.

Figure 5

A.

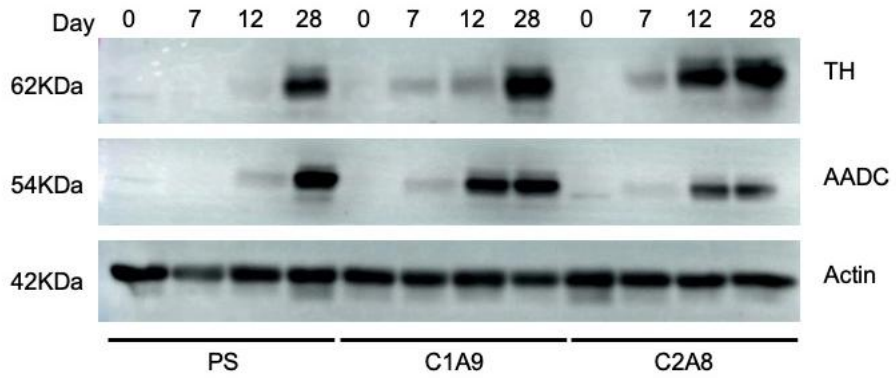

B.

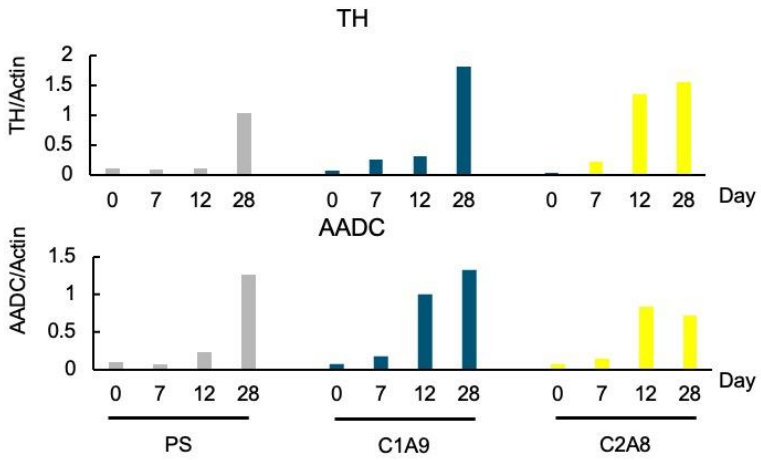

Figure 5 The expression level of protein in charged hydrogels induced DA neurons

(A)Protein levels analyzed by immunoblotting using antibodies against TH and AADC. Actin was used as a loading control. (B) The quantification of TH and AADC. It is shown in TH/Actin and AADC/Actin, respectively.

6. The TH-positive cells in charged hydrogels induced DA neurons

Next, I performed immunofluorescence analysis for TH on cells that had been cultured and induced to differentiate. Due to the challenges of immunostaining cells on gels, all samples were collected after differentiation and replated onto PS dishes

for staining. (Figure 6A) TH-positive cells were detected at 19.84% on PS dishes, compared to 43.05% on C1A9 gel and 41.67% on C2A8 gel, with a significant increase observed on both gels ($p<0.001$, $n=3$, respectively) (Figure 6B). These results indicate that DA differentiation of iPS cells was promoted on charged gels.

Figure 6

A

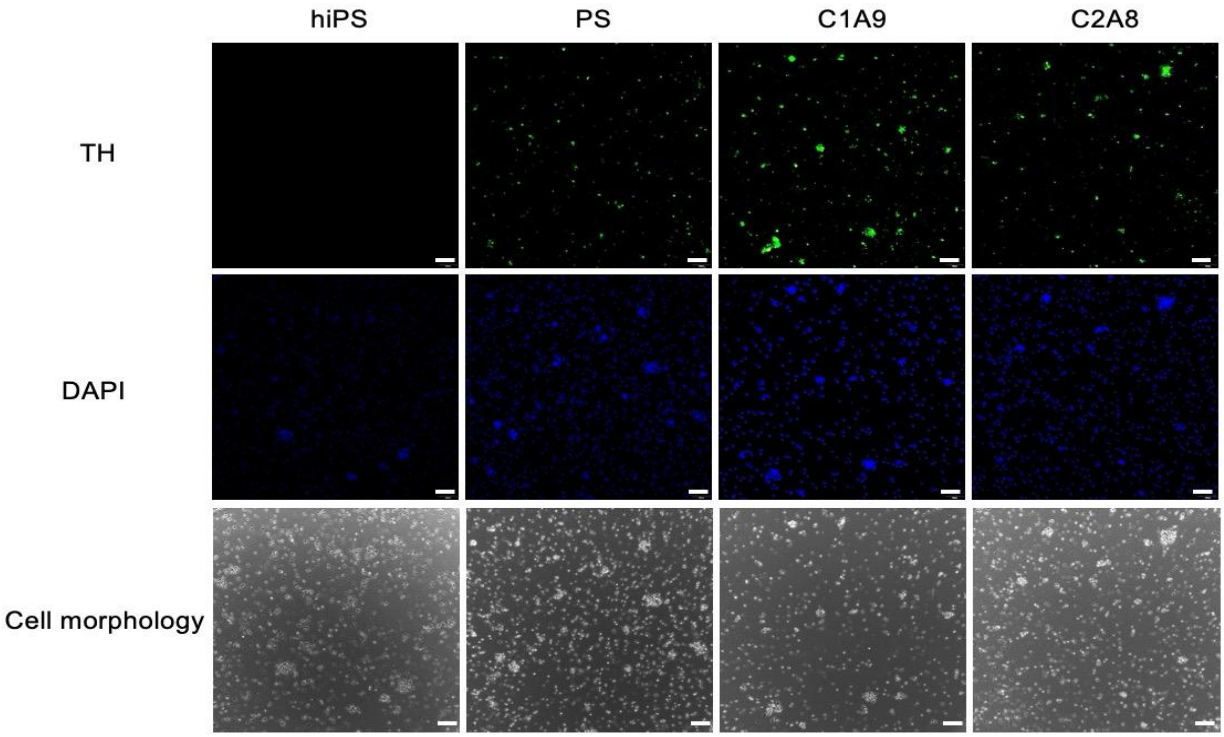

B.

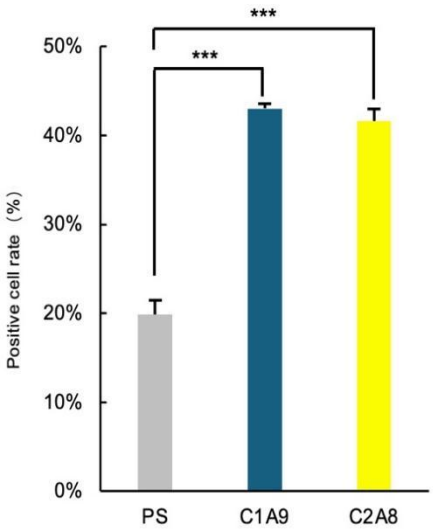

Figure 6 The TH-positive cells in charged hydrogels induced DA neurons

(A) Immunofluorescence analysis of TH (green) and DAPI (blue) in undifferentiated iPS cells and differentiated DA neurons on PS dish and charged hydrogels. Scale bars, 100 μm. The photographs are representative of n = 3 independent experiments with similar results. (B) The analysis of the positive cell rate of TH in the DA neurons. The data represent means ± s.d. (n = 3 independent experiments). Two-sided paired t-tests were used for statistical analysis. *P < 0.05; **P < 0.01; ***P < 0.001.

7. DA cells differentiated on charged gels show an early enhancement in dopamine production capacity.

Next, I examined the functionality of differentiated DA cells by assessing their L-dopa and dopamine production capabilities through *in vitro* experiments (Figure 7A) The concentrations of L-dopa and dopamine in the culture medium were measured using ELISA. The results were adjusted based on the total protein concentration in the cell lysate after harvesting, which reflects the cell count (Figure 7B). Following normalization, it could be described as:

$$\text{Normalized concentration} = \frac{\text{Original concentration} \times \text{Target cell number}}{\text{Sample cell number}}$$

After this, the concentrations of L-dopa in the culture medium were elevated on the charged gels at all stages measured from day 7 onward (Figure 7C). Dopamine levels were significantly elevated in the gel groups on day 28. Specifically, on day 7

of culture, the concentrations of L-dopa were 0.0017 ng/ml in the PS dish group, 10.62 ng/ml in the C1A9 group, and 13.16 ng/ml in the C2A8 group ($p<0.001$, n=3, respectively). On day 12, L-dopa concentrations were 11 ng/ml in the PS dish group, 40 ng/ml in the C1A9 group, and 60 ng/ml in the C2A8 group ($p<0.001$, n=3, respectively). By day 28, L-dopa levels reached 146 ng/ml in the PS dish group, 285 ng/ml in the C1A9 group, and 319 ng/ml in the C2A8 group ($p<0.001$, n=3, respectively). On the other hand, dopamine concentrations on day 7 were 15 pg/ml in the PS dish group, 75 pg/ml in the C1A9 group, and 198 pg/ml in the C2A8 group ($p>0.05$, n=3, respectively). By day 12, dopamine levels were 154 pg/ml in the PS dish group, 667 pg/ml in the C1A9 group, and 497 pg/ml in the C2A8 group ($p>0.05$, n=3, respectively). On day 28, dopamine concentrations reached 1522 pg/ml in the PS dish group, 3291 pg/ml in the C1A9 group, and 3810 pg/ml in the C2A8 group ($p<0.001$, n=3, respectively) (Figure 7C).

Figure 7

A.

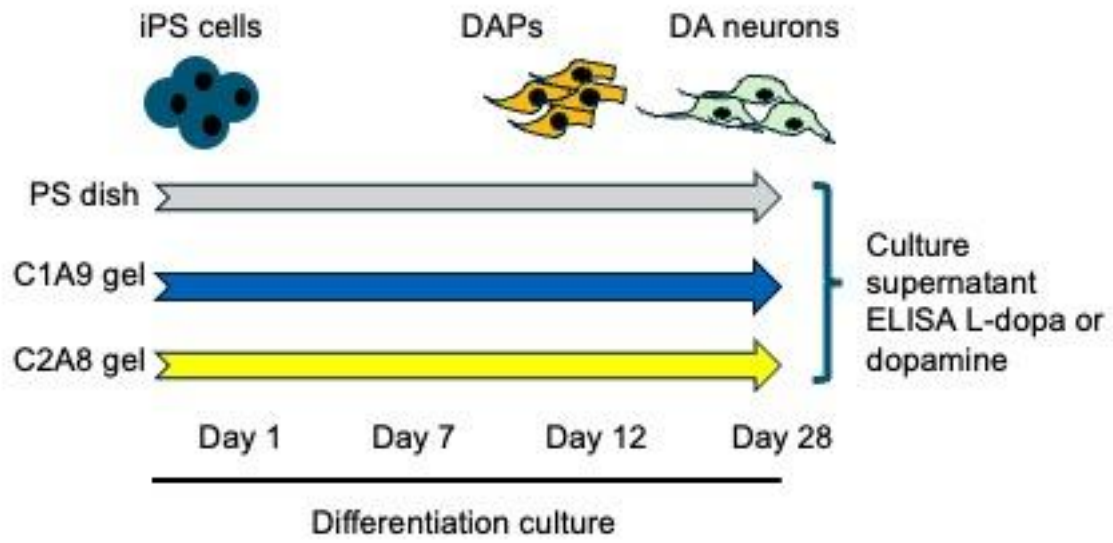

B.

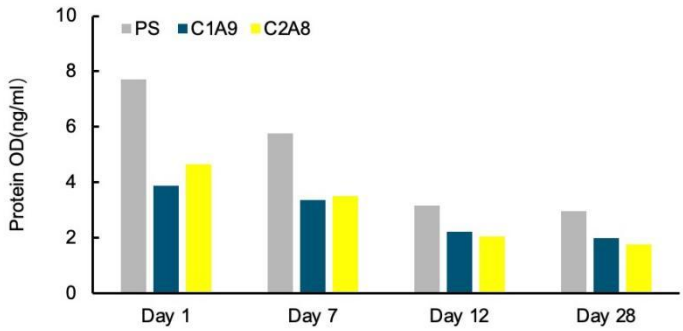

C.

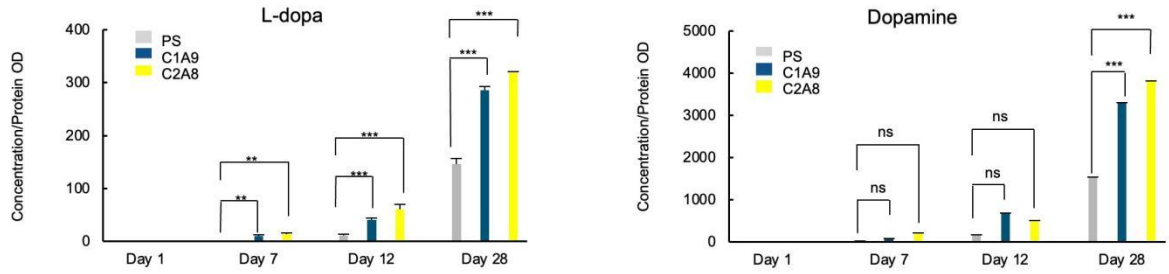

Figure 7 *In vitro* study on L-dopa and dopamine secretion from differentiated DA neurons

(A)The schema of *in vitro* assay. The conditioned medium was collected in day 1, day 7, day 12 and day 28. (B)Protein OD of cells on PS dish, C1A9 and C2A8 in day 1, 7, 12 and 28. (C) The concentration of L-dopa and dopamine from cells on PS dish, C1A9 and C2A8 in day 1, 7, 12 and 28 (n = 3 independent experiments). Two-sided paired t-tests were used for statistical analysis. P values for comparisons with the results for polystyrene dishes are indicated (*P < 0.05; **P < 0.01; ***P < 0.001).

8. *In vivo* study on L-dopa and dopamine secretion from differentiated DA neurons

Next, I performed an *in vivo* assay using mice. DA cells differentiated on each substrate were transplanted subcutaneously into rats at a concentration of 1×10^7 cells. Serum samples were collected on days 1, 3, 5, and 7, and the concentrations of L-dopa were measured using ELISA (Figure 8A). On day 1 post-injection, L-dopa concentrations were 320 ng/ml in the negative control group (no injection), 290 ng/ml in the PS dish group, 630 ng/ml in the C1A9 group, and 650 ng/ml in the C2A8 group ($p<0.001$, p value is the negative control group vs PS group, C1A9 group C2A8 group, n=3, respectively). On day 3, L-dopa levels were 330 ng/ml in the negative control group, 310 ng/ml in the PS dish group, 540 ng/ml in the C1A9 group, and 550 ng/ml in the C2A8 group ($p<0.001$, n=3, respectively). On day 5, the concentrations were 330 ng/ml for the negative control group, 360 ng/ml for the PS dish group, 450 ng/ml for the C1A9 group, and 470 ng/ml for the C2A8 group ($p<0.05$, n=3, respectively). By day 7, the L-dopa levels were 350 ng/ml in the negative control group, 320 ng/ml in the PS dish group, 450 ng/ml in the C1A9 group, and 470 ng/ml in the C2A8 group

($p<0.05$, n=3, respectively) (Figure 8B). Dopamine levels were checked only on day 3, and they also showed a significant increase in the gel groups (Figure 8C). These results suggest that the charged gels may stimulate the production and secretion of L-dopa and dopamine.

Figure 8

A.

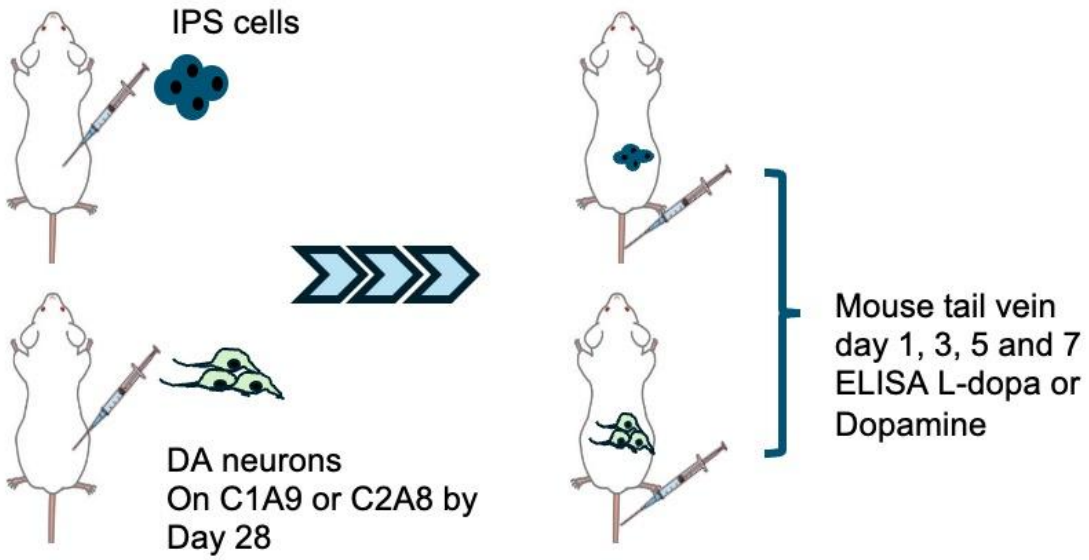

B.

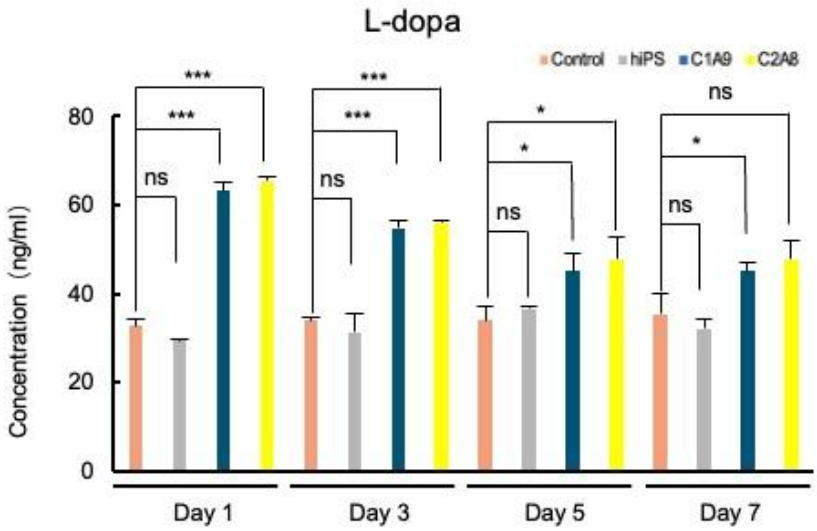

C.

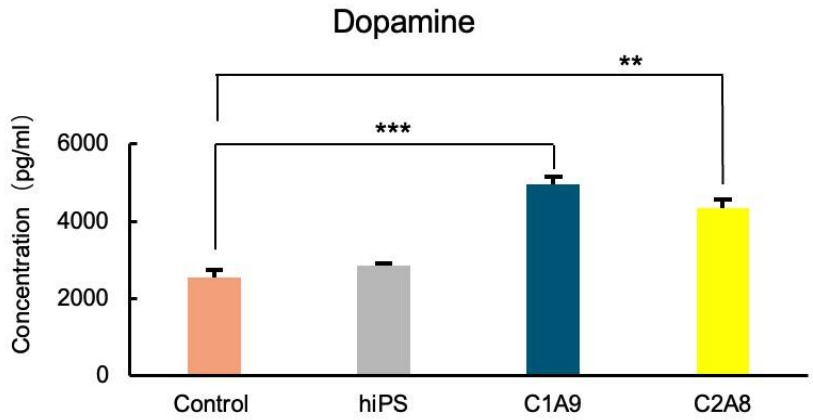

Figure 8 *In vivo* study on L-dopa and dopamine secretion from differentiated DA neurons

(A) The schema of *in vivo* assay. (B) The concentration of L-dopa in mice serum after the subcutaneously injection of differentiated DA neurons on PS dish, C1A9 and C2A8 in day 1, 3, 5 and 7. (C)Dopamine levels of mice serum after the injection of differentiated DA neurons on PS dish, C1A9 and C2A8 in day 3. Two-sided paired t-tests were used for statistical analysis. P values for comparisons with the results for polystyrene dishes are indicated (*P < 0.05; **P < 0.01; ***P < 0.001).

9. Transcriptome analysis revealed the activation of dopamine-related pathways in cells cultured on charged gels

RNA-sequence analysis was performed using four samples: undifferentiated control (hiPS_day 0) and differentiated samples on different scaffolds (PS_day28, C1A9_day28, and C2A8_day28) each with n=1. PCA results showed that all differentiated samples plotted away from the hiPS_day 0 control (Figure 9A). The hydrogels plotted closer together, but separately from PS_day28. Pairwise correlation analysis revealed a higher-than-expected correlation between the undifferentiated control and differentiated samples (Figure 9B, correlation coefficients: hiPS_day 0 vs. PS_day28, C1A9_day28, C2A8_day28 = 0.889, 0.874, 0.888). Pearson correlation coefficient among differentiated samples were even higher: PS_day28 vs. C1A9_day28 = 0.962, PS_day28 vs. C2A8_day28 = 0.967, and the hydrogels showed the highest correlation (0.982). Heatmap and clustering analysis demonstrated similar gene expression patterns between the hydrogels, distinct from those on PS dish (Figure 9C).

Figure 9

A.

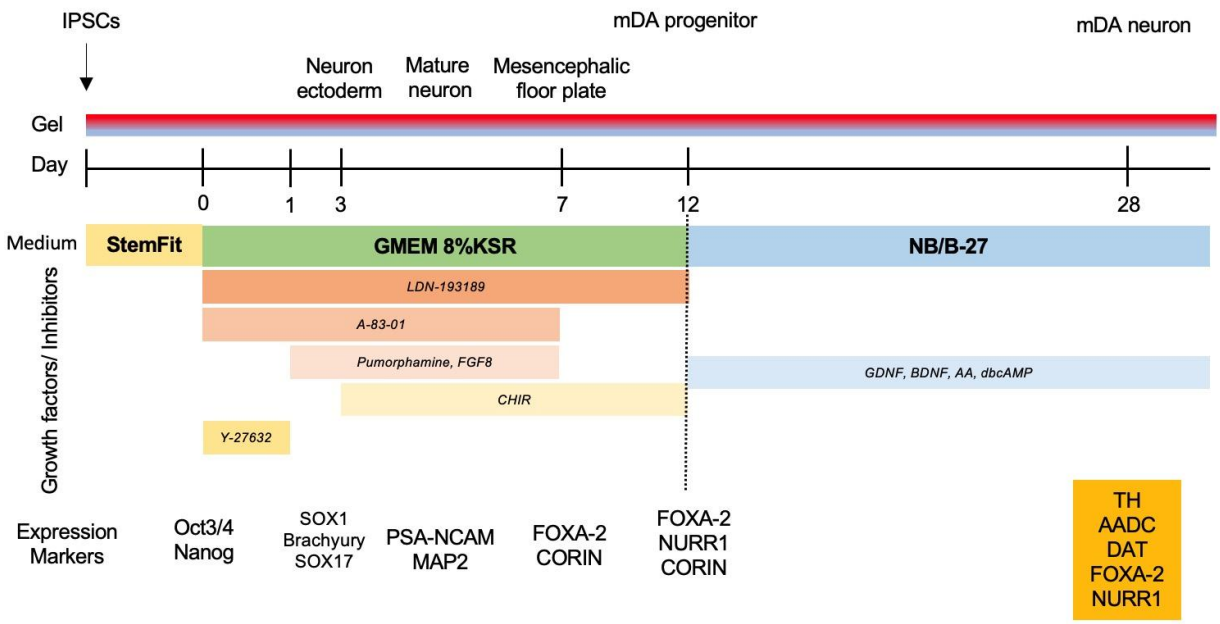

B.

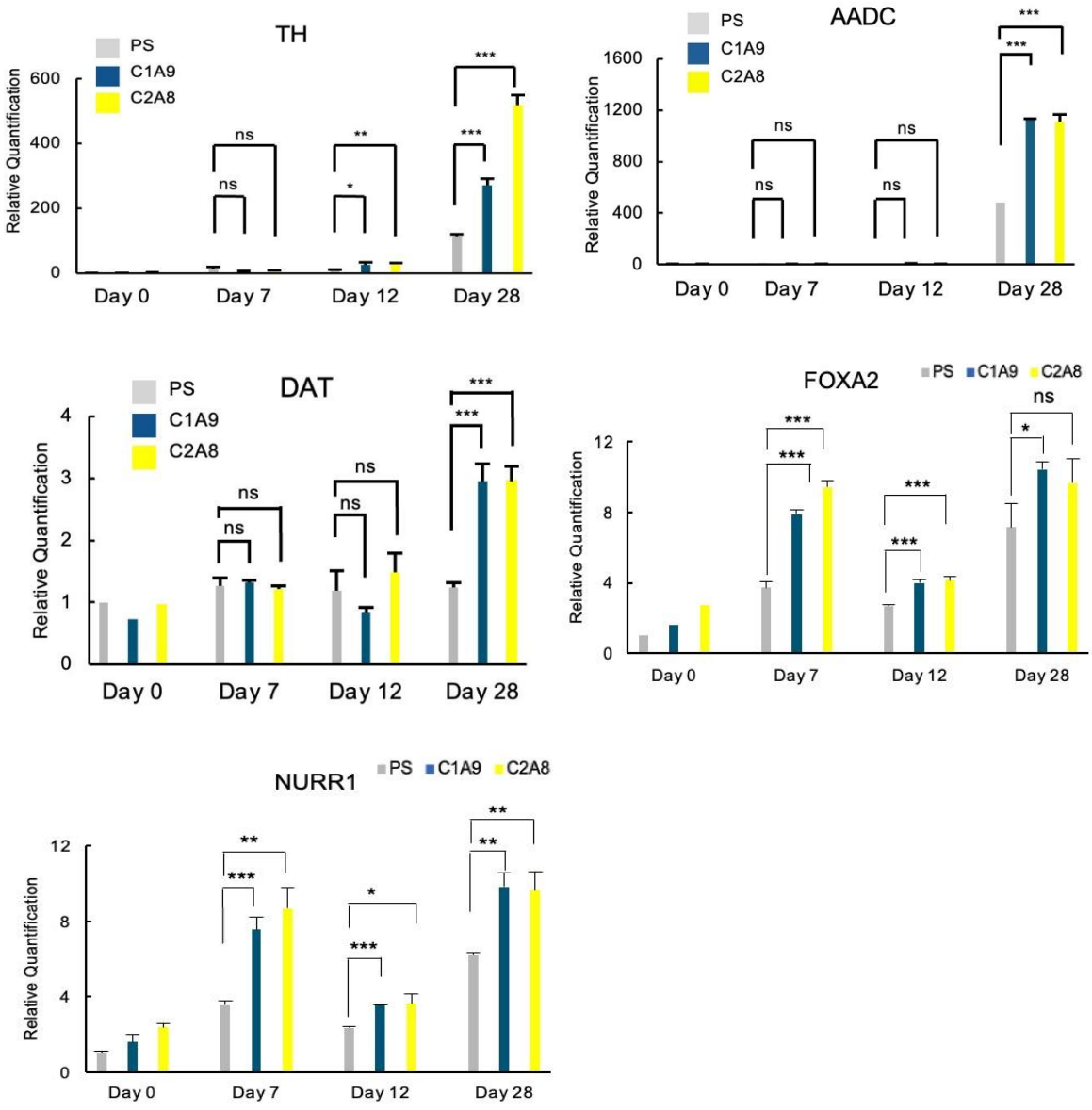
TH
PS
C1A9
C2A8
Relative Quantification
600
400
200
0
ns
ns
**
*
***
***
Day 0
Day 7
Day 12
Day 28
AADC
PS
C1A9
C2A8
Relative Quantification
1600
1200
800
400
0
ns
ns
ns
ns
***
***
Day 0
Day 7
Day 12
Day 28
DAT
PS
C1A9
C2A8
Relative Quantification
4
3
2
1
0
ns
ns
ns
ns
***
***
Day 0
Day 7
Day 12
Day 28
FOXA2
PS
C1A9
C2A8
Relative Quantification
12
8
4
0
***
***
***
***
ns
*
Day 0
Day 7
Day 12
Day 28
NURR1
PS
C1A9
C2A8
Relative Quantification
12
8
4
0
**
***
*
***
**
**
Day 0
Day 7
Day 12
Day 28

C。

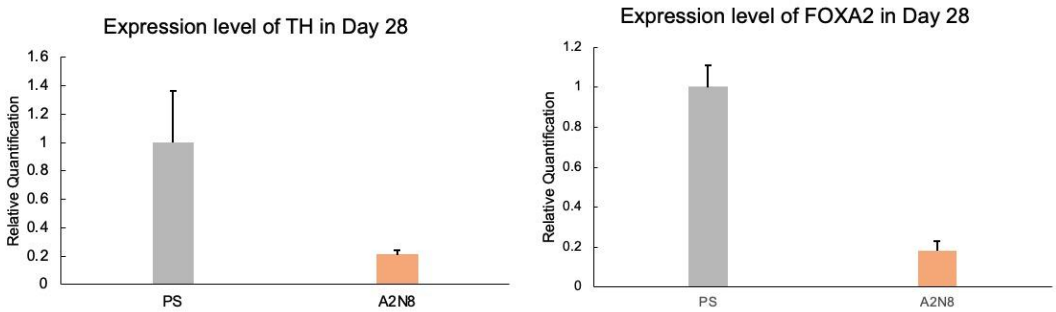

Figure 9 Comparative analysis of gene expression profiles across samples.
(A) Principal Component Analysis (PCA) plot showing the distribution of samples across the first two principal components. (B) Pairwise correlation matrix of gene expression profiles between different sample groups, visualized using scatter plots. The pearson correlation coefficient (Corr) is shown in each comparison, with asterisks indicating statistical significance (***$p < 0.001$). (C) Heatmap of hierarchical clustering analysis based on gene expression profiles across the four sample groups. The dendrograms represent the clustering relationships among the samples.

10. Transcriptome analysis of an increase in genes of cells cultured on charged gels

Next, I calculated the fold change by dividing the gene expression of each differentiated sample by that of the undifferentiated control. Genes with more than a two-fold increase were classified as upregulated: 5,533 in PS_day28, 7,041 in C1A9_day28, and 5,915 in C2A8_day28, with 3,949 genes commonly upregulated across the three groups (Figure 10A). DAVID analysis using GO on these commonly upregulated genes revealed 116 significant GO terms (adjusted p-value < 0.05). Treemap analysis using REVIGO of the BP GO terms showed broad inclusion of GO terms related to neuronal differentiation and synapse formation, including axon guidance (GO:0007411) (Figure 10B)

Figure 10

A.

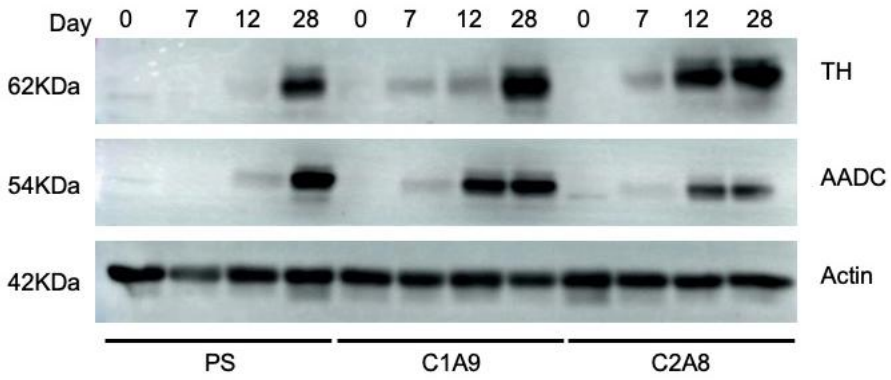

B.

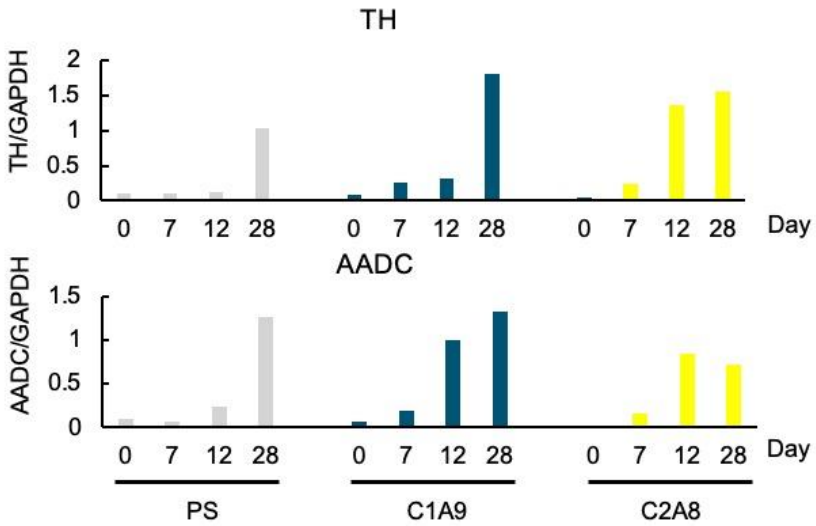

Figure 10 Comparative analysis of gene expression profiles across samples.

(A) Venn diagram displaying the overlap of upregulated genes between the differentiated samples. (B) Treemap showing GO terms significantly upregulated in all differentiated samples. GO terms are grouped into superclusters of loosely related terms, each visualized with a different color. The size of the rectangles reflects the p-value, with a representative GO term displayed in the center of each supercluster.

11. Transcriptome analysis of a decrease in genes of cells cultured on charged gels

On the other hand, genes with more than a two-fold decrease (downregulated genes) were as follows: 3,405 in PS_day28, 2,972 in C1A9_day28, and 3,067 in C2A8_day28, with 2,293 genes commonly downregulated across the three groups (Figure 11A). DAVID analysis on these commonly downregulated genes identified 143 significant GO terms (adjusted p-value < 0.05). REVIGO Treemap analysis of the BP GO terms revealed broad inclusion of GO terms related to cell division, including DNA replication (GO:0006260) (Figure 11B). These results indicate that the stem cell characteristics of hiPS_day0 were lost during differentiation, and neuronal differentiation was strongly promoted in all three groups.

Figure 11

A.

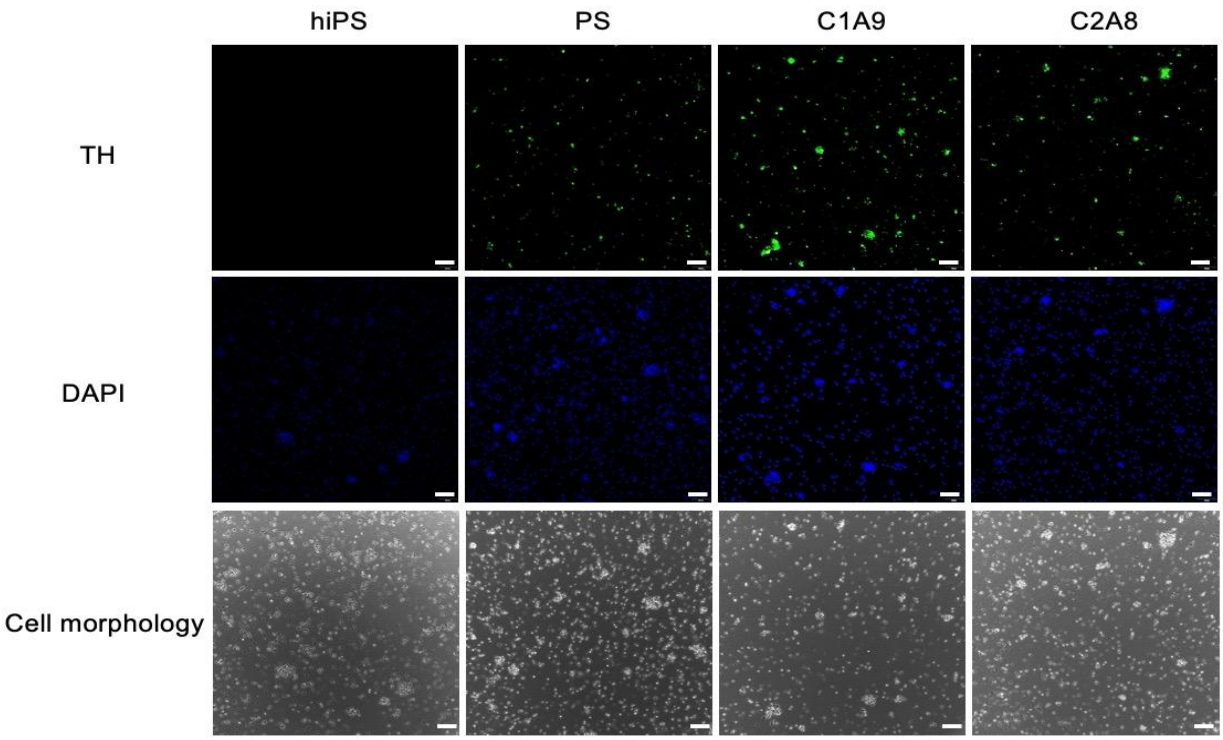

B.

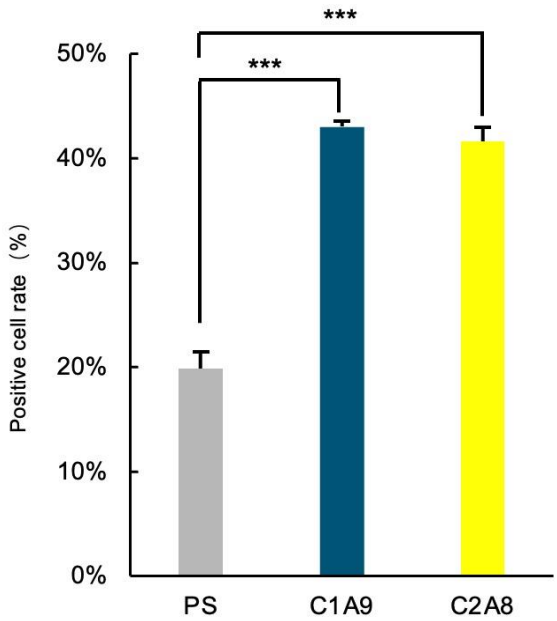

Figure 11 Comparative analysis of gene expression profiles across samples.
(A) Venn diagram showing the overlap of downregulated genes between the differentiated samples. (B) Treemap showing GO term significantly downregulated in all differentiated samples.

12. Transcriptome analysis revealed the activation of dopamine-related pathways in cells cultured on C1A9 gels

Next, a pre-ranked GSEA analysis was conducted to explore differences in gene expression profiles among the differentiated samples. To compare hydrogel and PS dish, PS_day28 was used as control and C1A9_day28 and C2A8_day28 genes were ranked by fold change.

GSEA analysis revealed 97 significant GO terms in C1A9_day28 (adjusted p-value < 0.05) (Figure 12A). Pathways significantly activated in C1A9 included many related to neuronal differentiation, particularly pathways associated with DA neurons, such as catecholamine secretion (GO:0050432) and dopamine transport (GO:0015872). Additionally, DAVID analysis using the gene list with more than a two-fold increase in C1A9_day28 identified 138 GO terms, which were visualized as

an interactive graph using REVIGO (Figure 12B). Similar to GSEA, DAVID analysis also highlighted GO terms related to neuronal differentiation and DA neurons.

Figure 12

A.

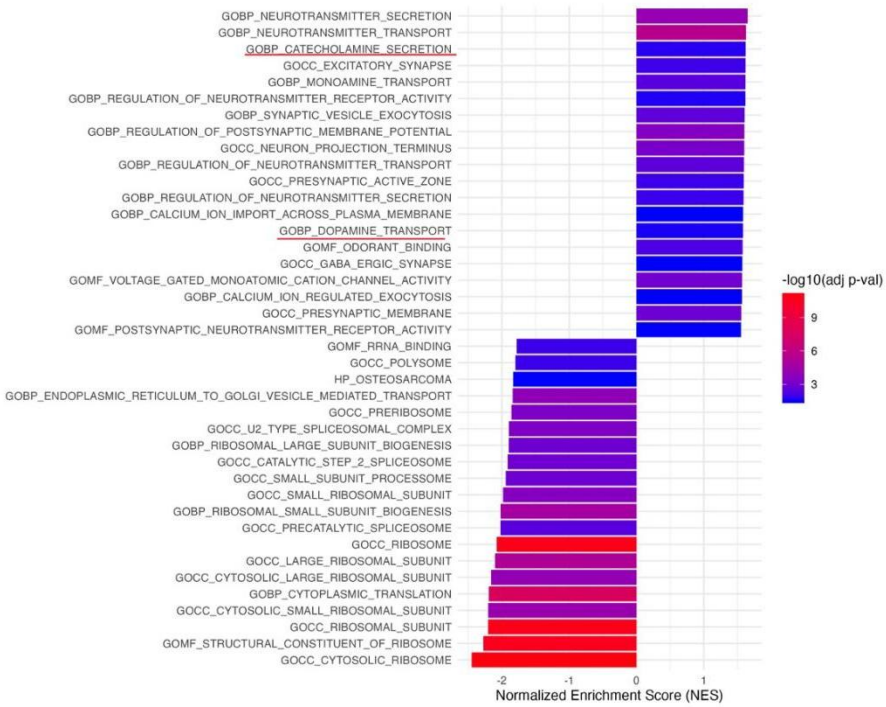

B.

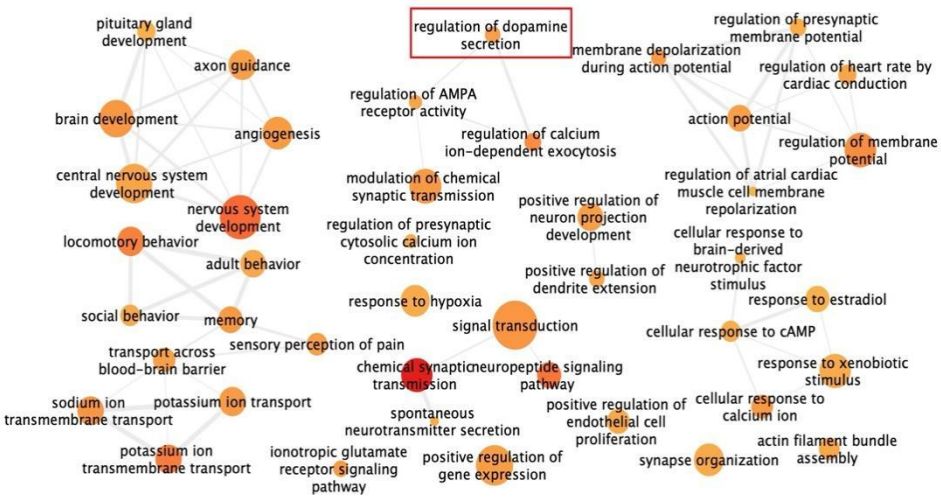

Figure 12 Pathway analysis between differentiated samples

(A) GSEA results for C1A9 vs. PS, showing the top enriched GO terms with their corresponding Normalized Enrichment Scores (NES). Bars are colored based on the -log10(p-value), indicating the significance of enrichment. The red underlines are GO terms involving DA neurons. (B) Interactive graph generated by REVIGO, illustrating the GO terms that are significantly upregulated in C1A9 compared to PS. Each node represents a GO term, with the size of the nodes proportional to the LogSize, reflecting the number of annotations associated with the GO term in the EBI GOA database. The color intensity of the nodes indicates the p-value, with darker shades representing more significant p-values. Edges between nodes indicate similarity between GO terms, with line thickness corresponding to the degree of similarity. The red squares are GO terms related to DA neurons.

13. Transcriptome analysis revealed the activation of dopamine-related pathways in cells cultured on C2A8 gels

A similar analysis was conducted for C2A8_day28. GSEA analysis identified 78 significant pathways (Figure 13A), showing a similar activation of neuronal differentiation pathways as in C1A9_day28. However, C2A8_day28 yielded higher rankings for GO terms related to DA neurons, such as catecholamine secretion (GO:0050432), dopamine transport (GO:0015872), and dopamine secretion (GO:0014046). DAVID analysis identified 90 GO terms, with neuronal differentiation and DA neuron-related GO terms confirmed in the interactive graph (Figure 13B). These results suggest that iPS cells induced to differentiate on hydrogels show more advanced neuronal differentiation and enhanced differentiation towards DA neurons.

Figure 13

A.

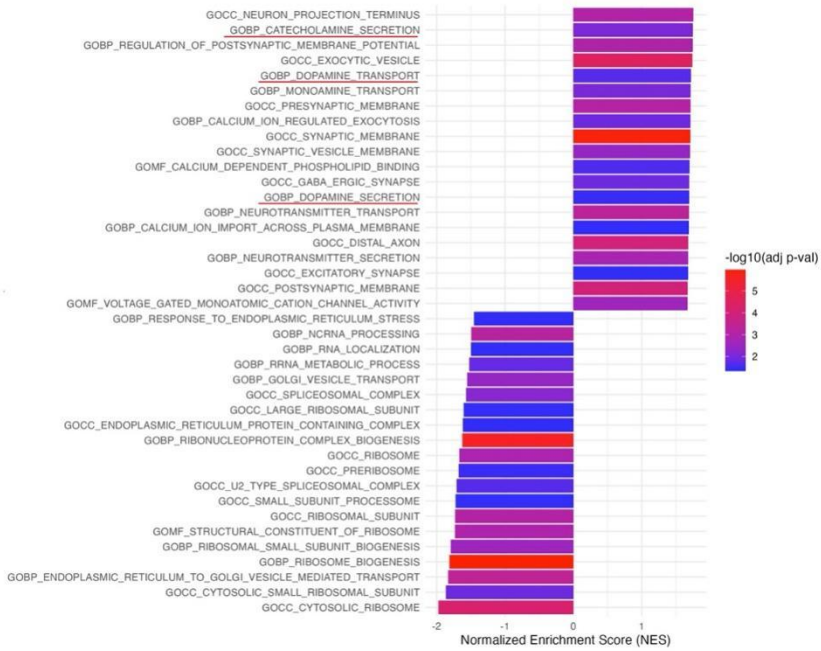

B.

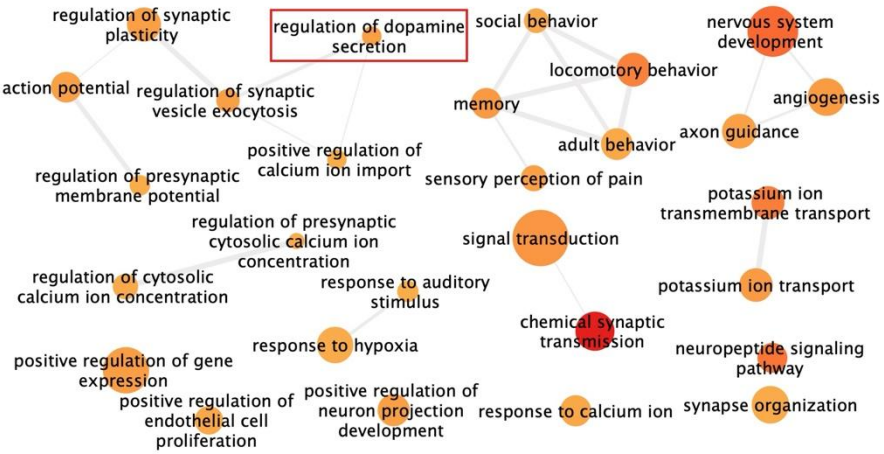

Figure 13 Pathway analysis between differentiated samples

(A) GSEA results for C2A8 vs. PS, showing the top enriched GO terms with their corresponding Normalized Enrichment Scores (NES). The red underlines are GO terms involving DA neurons. (B) Interactive graph created based on GO terms that are significantly activated by C2A8 compared to PS. The red squares are GO terms related to DA neurons.

14. The supplements of the mRNA sequence results by qPCR

qPCR was performed to support these results. Regarding dopamine transport (GO:0015872) and dopamine secretion (GO:0014046), Synaptotagmin-3/5/6 *(SYT3, SYT5* and *SYT6),* gamma-synuclein *(SNCG),* neuronal acetylcholine receptor subunit beta-2 *(CHRNB2),* cannabinoid receptor 1 *(CNR1),* gamma-aminobutyric acid B receptor 1 *(GABBR1),* dopamine receptor D1 *(DRD1)*, and dopamine receptor D2 *(DRD2)* were significantly upregulated in the gel groups (Figure 14).

Figure 14

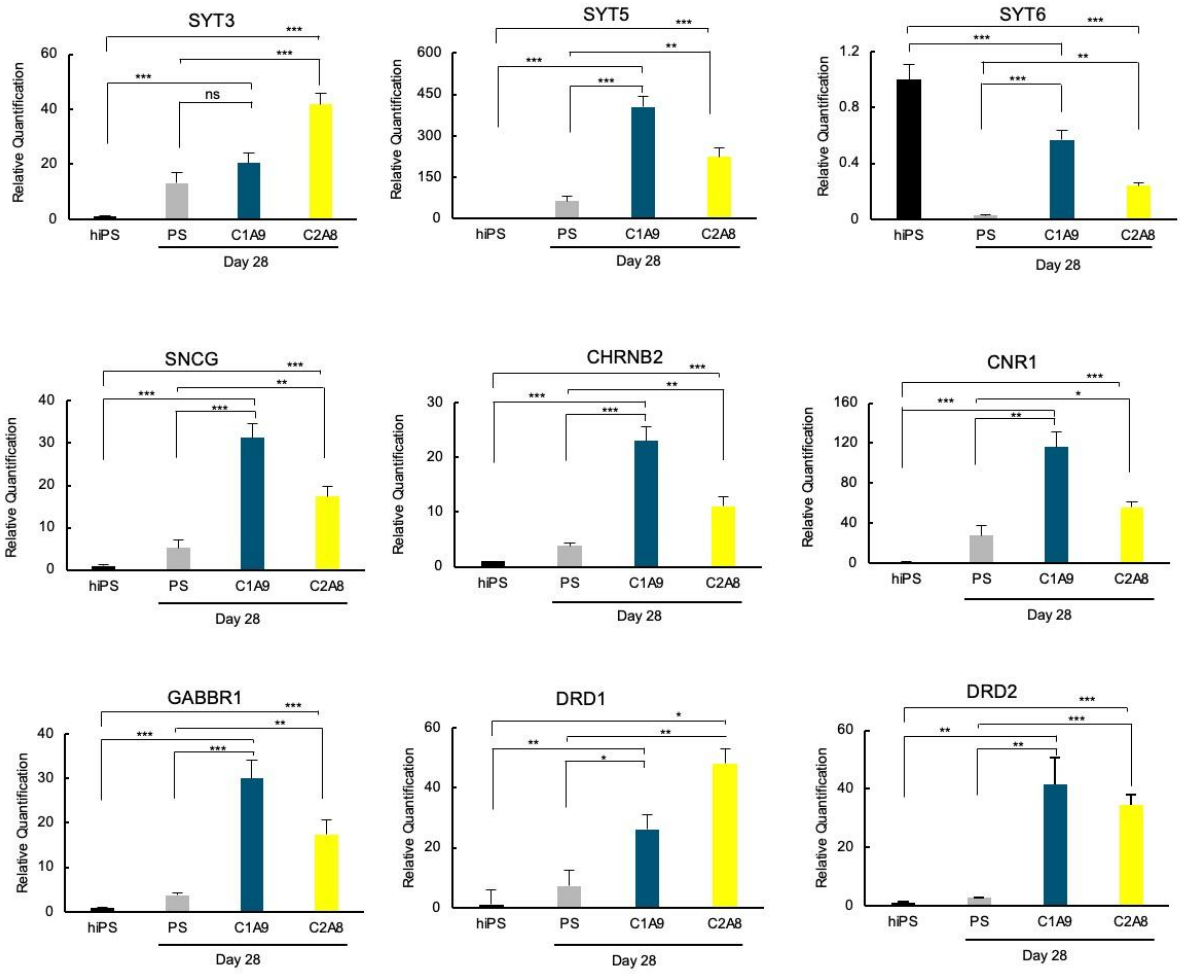

Figure 14 The supplements of the mRNA sequence result by qPCR. qPCR results for genes related to upregulated pathway (*SYT3, SYT5, SYT6, CNR1, GABBR1, SNCG, CHRNB2, DRD1* and *DRD2*). The data represent means ± s.d. (n = 3 independent experiments). Two-sided paired t-tests were used for statistical analysis. P values for

comparisons with the results for polystyrene dishes are indicated (*P < 0.05; **P < 0.01; ***P < 0.001).

15. The establishment of mice PD model

I administered the drug subcutaneously to the mice (Figure 15A). This time I made 2 kinds of mice PD model followed 20 mg/kg for 4 times with 2-h intervals as an acute model; 30 mg/kg/day for 5 days as a subacute model. And I only did the Footprint and Stepping Test this time (Figure 15B). The mice were divided into three groups (control group, acute group and subacute group), each group had the same condition.

In the Footprint and Stepping Test, Blume et al (Blume et al, 2009) found that MPTP decrease the length for a half to a third compared to the control mice. Stride width, usually 2~2.5 cm, is measured as the distance between the right and left footprint, which often increases in MPTP mice. Overlap, usually 0.5~0.7 cm, is measured as the distance between the center of front paw and hind paw footprints on the same side, which also increase in MPTP mice. However, in my thesis, the mice did not show any PD symptoms in the behavior after MPTP administration. There was no significant different between control group and acute/subacute group (Figure 15C). The reason might be:

1. Animal reasons, individual background differences between mice, different sensitivity to drugs, so lead to failure.

2. Insufficiently accurate drug dosage, or improper storage of the drug makes the drug ineffective.

3. Improper operation when injecting the drug into the mice, resulting in the mice receiving accidental injuries or being in a strong state of stress, causing the experiment to fail.

4. Waiting for the drug to take effect for a certain period of time after the drug has been administered, but too long or too short a period of time will cause poor results in the measurement.

Namely, there is still have improvement rooms in the further research.

Figure 15

A.

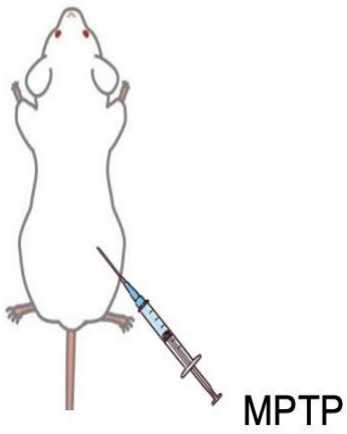

B.

C.

Control group mice

Acute group mice

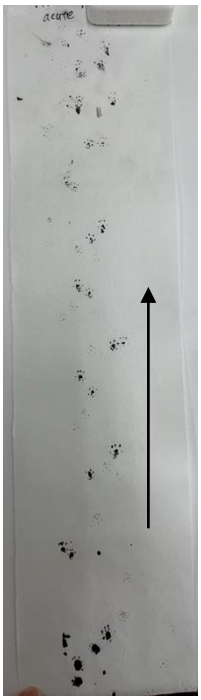

Subacute group mice

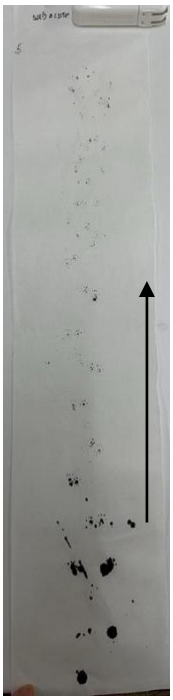

Figure 15 The establishment of mice PD model

(A)20 mg/kg and 30mg/kg for 4 times with 2h intervals as an acute model, 30 mg/kg/day for 5 days as a subacute model, injected into the subcutaneous of the C57BL/6JJcl mice. (B)The result of Footprint test after the administration of MPTP. There was no significant different between control group and acute/subacute group. (Left: control group, Mid: acute group, Right: subacute group)

Discussion

The most significant differences between the hydrogel and PS dish are surface charge and stiffness. I developed a kind of new hydrogel which is not expensive and the hydrogel is considerably softer than the PS dish. Previous studies have shown that substrates with varying stiffness can promote neuronal differentiation (Engler AJ et al, 2006). In this thesis, I observed an early promotion of neural differentiation on the hydrogel compared to the PS dish, suggesting that substrate stiffness may have influenced this outcome. Additionally, surface charge may provide distinct stimuli to adherent cells by affecting protein adsorption from the culture medium or proteins secreted by the cells, or by directly influencing membrane potential. The effectiveness of cell adhesion systems using cationic gels has also been highlighted in other studies (Stamm N et al, 2022). In this work, I developed the hydrogel system to investigate the concentration-dependent effect of cationic and anionic charge on the behavior of human iPS cells in 2D cultures. Previous studies have already demonstrated the importance of charge in supporting cell adhesion (Hynes SR et al, 2009; Cai L et al, 2012; Cai L et al, 2012; Sallouh M et al, 2017). However, the immunofluorescence analysis showed that increasing concentrations of cationic molecules led to not only more live cells adhering to the gel surface but also an increase in dead cells. The ratio of live to dead cells clearly indicated an optimum concentration of cationic charge, where the number of living cells was high with a minimal number of dead cells. This is unsurprising as numerous studies have suggested that amino groups and excessive cationic charge may be toxic to cells (Fischer D et al, 2003; Dekie L et al, 2000).

The stiffness and charge promoted the differentiation of iPS cells into DA neurons; however, the limitation is that specific mechanisms remain unclear. In discussing the differences due to charge, it is interesting to note that in the hydrogel A2N8, composed of anionic and neutral monomers, there was no observed increase in mRNA expression levels of *TH*, a marker of DA cells. This suggests that even among similarly soft hydrogel substrates, differences in surface charge can influence the differentiation fate of the cells. Although C10N0, C3N7, etc. have less modulus, the excessive of cationic charge may be toxic to cells (Fischer D et al, 2003; Dekie L et al, 2000). Namely, only have the suitable cationic and anionic charge could induce cells efficiently.

On the other hand, different kinds of hydrogel could promote the differentiation of cells. And it is known that surface charge and wettability of artificial substrate could contributed to cell adhesion on scaffold, and surface charge of the substrates may

directly affect adhesion of cellular membrane proteins. The electrical charge of the substratum in the context of cellular adhesion, that is electrical charged hydrogels could effectively reprogram cells by changing their adhesion and cellular membrane proteins (Wang Y et al, 2019; Martin Frauenlob et al, 2019; Suzuka J et al, 2022). Another approach to improving differentiation protocols involve the properties of the culture substrate. Surface charge, stiffness and wettability of artificial substrate contribute to cell adhesion, and substrate surface charge may directly affect adhesion of cellular membrane proteins. Manish Ayushman (Ayushman M et al, 2024) found that different hydrogels have various substrates that could influence cell tumbling (a whole-cell movement that occurs on sliding hydrogels over a short timescale) to enhance the differentiation. Xun Xu et al. (Xu X et al, 2024) showed that blastocyst motif substrates could revert pluripotent stem cell to naive state. Furthermore, Gaspard Pardon et al. (Pardon G et al, 2024) demonstrated that substrate stiffness affects the differentiation of cardiomyocytes in their study of CONTRAX, a pipeline for tracking the contractile dynamics of single iPS cells-derived cardiomyocytes. Hydrogels are promising soft materials as tissue engineering scaffolds, stretchable sensors, and soft robotics. Their mechanical flexibility, structural permeability, and biocompatibility make them ideal for constructing soft electronics and biomedical devices.

In this thesis, two kinds of electrically charged hydrogels were found, which composed of cationic and anionic monomers in 1:9 and 2:8 ratio, were suitable for the attachment, growth, and differentiation of DA neurons. Furthermore, DA neurons differentiated in these gels led to effective survival, migration, and differentiation.

Furthermore, GSEA analysis revealed activation of various pathways, in addition to promoting DA neuron differentiation. While many pathways were shared between the C1A9 and C2A8 hydrogels, differences were particularly observed in ribosome-related pathways when comparing the two (data not shown). These pathway differences may reflect the variations in charge between the hydrogels.

In this experiment, I injected the DA neurons generated by gel-induced differentiation into mice and detected higher levels of L-dopa and dopamine in the serum of the mice. However, as I know, dopamine cannot pass through the BBB, so the only make more L-dopa (which passes through the BBB) could generate more dopamine.

The survival duration of transplanted iPS cells is one important standard for the effect of the cell transplant. However, few papers reported it in their research. In their

paper (Doi D et al 2020), the only showed the symptom of the PD model or patient has been improved significantly after the transplantation, but did not show the survival duration of transplanted cells. The subjects' PD symptoms continued to improve for at least 24 months after transplantation.

Of course, the transplanted cells cannot 100% survive and the decline in cell viability may be causing a decrease in concentration over time. That time, I will include a tissue image evaluation of the transplant site in my future research. It is also necessary to consider an appropriate transplant site (intramuscular, subcutaneous, the digestive tract, etc., which has many L-dopa transporters).

Currently, the standard treatment is to administer L-dopa from the periphery, and transplantation of DA cells into the brain is the mainstream of research, but as a future plan, I am exploring a treatment method to substitute for drug administration by transplanting L-dopa-producing cells into peripheral tissues. For this reason, I attempted peripheral transplantation this time.

The interview form of Dopaston® (CADTH, 2018) described that C_{max} of L-dopa after the administration of L-dopa was more than 3000ng/mL and EC_{50} was 640ng/mL, however, in my thesis, it was only 60ng/mL, this is also linked to the issue of survival rate, and the appropriate number of transplanted cells is not clear at this time. At this time, the concentration is clearly low, in the future research, the amount must be considered using a disease model along with the transplant site. That time, the effect of increasing the baseline L-dopa can be expected.

In the research of Doi D (Doi D et al 2020), they reported that teratoma is one of the major problems in iPS cells transplantation. In order to avoid this, they used the cell sorting. In my thesis, because the reason of antibody and the growth characteristics of iPS cells, cell sorting could not be done in my research, however, in my data, it was showed that the expression level of *TH,* TH-positive rate was higher compared to the PS dish group, and on the other hand, Razan Sheta (Razan Sheta et al, 2022) showed the cell sorting is not the golden standard for the differentiation of DA neurons. So, regarding to teratoma, it could be generated from the undifferentiated iPS cells and in my research, I have not confirmed the number of undifferentiated cells, however, in the research data especially in the mRNA-sequence analysis, it clearly shows that the undifferentiated components decrease early when differentiation is induced using hydrogel. However, in my future plan, I will use cell sorting to avoid the undifferentiated cells. I would like to induce DA neurons on hydrogels, by co-culturing with a porous gel, it will be possible to maintain DA

neurons for a long time *in vivo*, and then before transplantation, using cells sorting to screen out the undifferentiated cells. So that, it is possible to remove the risks from it.

The DA neuron markers such as *TH, AADC* and *DAT* could reflect the differentiation of it. In my data, it showed these markers was promoted significantly. On the other hand, the vesicular monoamine transporter (*VMAT2*) has the similar function of DAT which are regulated by complex processes such as phosphorylation, protein–protein interactions, and changes in intracellular localization. *VMAT2* synaptic vesicle localization within presynaptic terminals can play an important role in monoamine uptake. Similar to *DAT*, *VMAT2*-mediated monoamine transport is regulated by post-translational modification, protein interactions, and presynaptic localization, although less is known about these processes. *VMAT2* has been assumed to follow stages of the synaptic vesicle cycle in a manner similar to other neurotransmitter systems. In the midbrain, *VMAT2* is internalized and vesicles are reformed faster, segregate to different terminal and axonal locations, and release at a lower rate than vesicles associated with the vesicular glutamate transporter (Onoa et al., 2010). The post-translational modifications, protein interactions, and sorting patterns of *VMAT2* likely underlie the unique way in which these vesicles engage the synaptic vesicle cycle, as well as their response to different pharmacologic agents. The expression level of *VMAT2* will be checked in my further research.

In this thesis, L-dopa concentration on day 7 was lower than that on day 1(Figure 8), it suggested that the survival rate of the transplanted iPS cells was not high. The reason might be:

1. Immune rejection:

When DA neurons are transplanted into the mice, the immune system of mice may recognize these cells as foreign and initiate an immune response to reject them. This rejection can lead to the death of the transplanted cells and trigger a systemic immune response, potentially resulting in this result.

2. Injury or inadaptability of the transplanted cells:

Transplanted DA neurons may be damaged during the procedure or by stress factors, such as temperature fluctuations or suboptimal culture conditions. If the transplanted cells cannot adapt to the new physiological environment, they may undergo apoptosis or die.

3. DA neurons quality issues:

The quality of neurons directly impacts the success of transplantation.

4. Nutritional and environmental factors after transplantation:

After transplantation, the cells may face environmental mismatches (such as temperature, pH, or electrolyte imbalances) and nutritional deficiencies, which can affect cell survival and function. If the conditions are not optimal, the DA neurons may undergo stress responses or die.

In further research, I intend to implant the DA neurons induced by iPS cells to the midbrain and the terminal organization of PD animal model, let the DA neurons in the midbrain to generate more dopamine. At the same time, the DA neurons in the terminal organization could generate more L-dopa, namely, it is a development of a method to induce DA activity more efficiently than before.

On the other hand, for animal models modeling failures may be these causes:

1. Animal reasons

The experimental animals are in suboptimal health or infected, it may compromise the establishment of the model and the reliability of the results.

2. Technical issues in procedure

Inaccurate modeling methods: different disease models require specific procedures. Improper technique, such as incorrect drug administration, dosage, or timing, may lead to failure this time.

Improper handling or equipment issues: incorrect surgical techniques (e.g., infection or excessive trauma) or inadequate equipment (e.g., unclean syringes or drug preparation tools) can also contribute to failure.

Incorrect induction timing: certain disease models require precise timing for induction. If the timing is too long or too short, the model may not develop as expected.

3. Issues with dosage and drugs

Incorrect drug dosage: using excessively high or low doses of drugs can result in the failure of the model. Drug solubility, stability, and delivery accuracy may also affect the outcome.

Drug purity: low purity or contaminants in the drugs used can impact the success of the modeling process.

Inappropriate drug administration: choosing the wrong route of drug administration can lead to suboptimal effects, impacting the disease model's establishment.

4. Environmental factors

Suboptimal environmental conditions: factors like temperature, humidity, and light cycle can significantly affect the health and well-being of animals. If these

environmental conditions are not carefully controlled, animal health may be compromised, leading to failed experiments.

Improper animal care: poor diet, water quality, or sanitation can influence the animals' health and experimental outcomes. Inadequate animal care may result in immune system impairment or poor general health, which affects the modeling process.

5. Adaptive responses

Stress responses: stress induced by handling, environmental changes, or experimental procedures can affect the physiological state of animals, leading to modeling failure.

6. External contamination

Environmental contamination: contamination from the laboratory air, drinking water, or feed can negatively impact animal health, thereby affecting the outcomes of the experiment.

In summary, I found that the C1A9 and C2A8 gels could induce the differentiation of DA neurons more efficiency, and this phenomenon may be referred to as hydrogel-activated promotion.

There is growing anticipation for cell transplantation in PD, emphasizing the importance of developing methods to efficiently generate DA cells. I have revisited DA cell differentiation from the perspective of substrate properties and identified improved conditions. These findings provide new insights into the generation of DA cells.

Conclusion

In summary, I found that the C1A9 and C2A8 gels could induce the differentiation of DA neurons more efficiency, and this phenomenon may be referred to as hydrogel-activated promotion.

1. On C1A9 and C2A8 hydrogels, cell attachment and proliferation were observed. Following seeding on C1A9 and C2A8, cells could aggregate and make clusters.

2. The DA cell differentiation markers (*TH*, *DAT* and *AADC*), neural differentiation markers (*PSA-NCAM* and *MAP2*), midbrain differentiation markers (*CORIN*, *NURR1* and *FOXA2*) had a significant increase in the gel group compared to the PS group.

3. In day 28, the expression level of protein of TH and AADC were increased in both gels. At the same time, the TH-positive cells had a significant increase observed on both gels.

4. *In vitro* and *in vivo* study on L-dopa and dopamine secretion from differentiated DA neurons, an increase was observed in gel groups.

5. mRNA sequence analysis suggested that iPS cells induced to differentiate on hydrogels show more advanced neuronal differentiation and enhanced differentiation towards DA neurons. On the other hand, qPCR was performed to support these results.

One limitation of this study is that the essential chemical and/or physical factor(s) of the C1A9 and C2A8 gels were not directly described and 100% precisely controlled, so further study is required.

Acknowledgements

This study was supported in part by Japan China Sasakawa Medical Fellowship. This work is supported by grants from MEXT (19H01171 to S.T., and 15K15106), and AMED (A171 to Satoshi Tanikawa, 20cm0106571h0001 and 21cm0106571h0002 to Shinya Tanaka). The Institute for Chemical Reaction Design and Discovery (ICReDD) was established by the World Premier International Research Center Initiative (WPI), MEXT, Japan.

Disclosure of Conflict of Interest

The author declares no conflict of interest.

References

1. Alekseenko Z, Marklund U, Kjellander S, Volakakis N, Hovatta O, El Manira A, Björklund A, Perlmann T, Ericson J (2009). Efficient production of mesencephalic dopamine neurons by Lmx1a expression in embryonic stem cells. Proc Natl Acad Sci U S A. May 5;106(18):7613-8.
2. Ayushman M, Mikos G, Tong X, Sinha S, Lopez-Fuentes E, Jones S, Pamela C Cai, Hung-Pang Lee, Morrison AJ, Spakowitz A, et al (2024). Cell tumbling enhances stem cell differentiation in hydrogels via nuclear mechanotransduction. Nat. Mater. Nov 1. doi: 10.1038/s41563-024-02038-0.
3. Barbeau A, Dallaire L, Buu NT, Veilleux F, Boyer H, de Lanney LE, Irwin I, Langston EB, Langston JW (1985). New amphibian models for the study of 1-methyl-4-phenyl-1,2,3,6-tetrahydropyridine (MPTP). Life Sci. Mar 18;36(11):1125-34.
4. Betarbet R, Sherer TB, Greenamyre JT (2002). Animal models of Parkinson's disease. Bioessays. Apr;24(4):308-18.
5. Braungart E, Gerlach M, Riederer P, Baumeister R, Hoener MC (2004). Caenorhabditis elegans MPP+ model of Parkinson's disease for high-throughput drug screenings. Neurodegener Dis.1(4-5):175-83.
6. Blume, S.R., Cass, D.K., Tsueng, K.Y., (2009). Stepping test in mice: a reliable approach in determining forelimb akinesia in MPTP-induced Parkinsonism. Exp. Neurol. 219, 208–211.
7. Chambers SM, Fasano CA, Papapetrou EP, Tomishima M, Sadelain M, Studer L (2009). Highly efficient neural conversion of human ES and iPS cells by dual inhibition of SMAD signaling. Nat Biotechnol. Mar;27(3):275-80.
8. Choudhury ME, Moritoyo T, Yabe H, Nishikawa N, Nagai M, Kubo M, Matsuda S, Nomoto M (2010). Zonisamide attenuates MPTP neurotoxicity in marmosets. J Pharmacol Sci.;114(3):298-303.
9. C.T. McKee, J.A. Last, P. Russell, C.J. Murphy (2011). Indentation Versus Tensile Measurements of Young’s Modulus for Soft Biological Tissues, Tissue Eng. Part B Rev. 17 155–164.
10. Choi CB, Kim SY, Lee SH, Jahng GH, Kim HY, Choe BY, Ryu KN, Yang DM, Yim SV, Choi WS (2011). Assessment of metabolic changes in the striatum of a MPTP-intoxicated canine model: in vivo ^{1}H-MRS study of an animal model for Parkinson's disease. Magn Reson Imaging. Jan;29(1):32-9.

11. Cai L, Lu J, Sheen V, Wang S (2012). Promoting nerve cell functions on hydrogels grafted with poly(L-lysine). Biomacromolecules. Feb 13;13(2):342-9.
12. Cai L, Lu J, Sheen V, Wang S (2012). Optimal poly(L-lysine) grafting density in hydrogels for promoting neural progenitor cell functions. Biomacromolecules. May 14;13(5):1663-74.
13. Crowley J (2024). GGally: Extension to 'ggplot2'. R package version 2.2.1, https://github.com/ggobi/ggally, https://ggobi.github.io/ggally/. (2024 年 11 月 19 日参照)
14. Dekie L, Toncheva V, Dubruel P, Schacht EH, Barrett L, Seymour LW (2000). Poly-L-glutamic acid derivatives as vectors for gene therapy. J Control Release. Mar 1;65(1-2):187-202.
15. Davie CA (2008). A review of Parkinson's disease. Br Med Bull. 86:109-27.
16. Doi D, Samata B, Katsukawa M, Kikuchi T, Morizane A, Ono Y, Sekiguchi K, Nakagawa M, Parmar M, Takahashi J (2014). Isolation of human induced pluripotent stem cell-derived dopaminergic progenitors by cell sorting for successful transplantation. Stem Cell Reports. Mar 6;2(3):337-50.
17. Doi D, Magotani H, Kikuchi T, Ikeda M, Hiramatsu S, Yoshida K, Amano N, Nomura M, Umekage M, Morizane A, et al (2020). Pre-clinical study of induced pluripotent stem cell-derived dopaminergic progenitor cells for Parkinson's disease. Nat Commun. Jul 6;11(1):3369.
18. Engler AJ, Sen S, Sweeney HL, Discher DE (2006). Matrix elasticity directs stem cell lineage specification. Cell. Aug 25;126(4):677-89.
19. Fischer D, Li Y, Ahlemeyer B, Krieglstein J, Kissel T (2003). In vitro cytotoxicity testing of polycations: influence of polymer structure on cell viability and hemolysis. Biomaterials. Mar;24(7):1121-31.
20. Friling S, Andersson E, Thompson LH, Jönsson ME, Hebsgaard JB, Nanou E, Kirkeby A, Grealish S, Wolf DA, Nelander J, et al (2012). Generation of regionally specified neural progenitors and functional neurons from human embryonic stem cells under defined conditions. Cell Rep. Jun 28;1(6):703-14.
21. Frauenlob M, Kurokawa T, Kojima S, Ueno T, Ohmiya Y, Mano H, Yasuda K, Gong JP, Tanaka S (2021). Rapid reprogramming of tumour cells into cancer stem cells on double-network hydrogels. Nat Biomed Eng. Aug;5(8):914-925.
22. Ghribi O, Herman MM, Pramoonjago P, Savory J (2003). MPP+ induces the endoplasmic reticulum stress response in rabbit brain involving activation of the

ATF-6 and NF-kappaB signaling pathways. J Neuropathol Exp Neurol. Nov;62(11):1144-53.

23. Gupta HV, Lyons KE, Wachter N, Pahwa R (2019). Long Term Response to Levodopa in Parkinson's Disease. J Parkinsons Dis.9(3):525-529.
24. Gao CH, Yu G, Cai P (2021). ggVennDiagram: An Intuitive, Easy-to-Use, and Highly Customizable R Package to Generate Venn Diagram. Frontiers in Genetics 12, 1598.
25. Gao CH, Chen C, Akyol T, Duşa A, Yu G, Cao B, Cai P (2024). ggVennDiagram: intuitive Venn diagram software extended. iMeta 3, 69.
26. Harris MK, Shneyder N, Borazanci A, Korniychuk E, Kelley RE, Minagar A (2009). Movement disorders. Med Clin North Am. Mar; 93(2):371-88.
27. Hynes SR, Rauch MF, Bertram JP, Lavik EB (2009). A library of tunable poly (ethylene glycol)/poly(L-lysine) hydrogels to investigate the material cues that influence neural stem cell differentiation. J Biomed Mater Res A. May; 89(2):499-509.
28. Jiang S, Wang H, Yang C, Feng F, Xu D, Zhang MZ, Xie MQ, Cui RX, Zhu ZZ, Jia CH, et al (2024). Phase 1 study of safety and preliminary efficacy of intranasal transplantation of human neural stem cells (ANGE-S003) in Parkinson's disease. J Neurol Neurosurg Psychiatry.95(12):1102-1111.
29. Kalaria RN, Mitchell MJ, Harik SI (1987). Correlation of 1-methyl-4-phenyl-1,2,3,6-tetrahydropyridine neurotoxicity with blood-brain barrier monoamine oxidase activity. Proc Natl Acad Sci U S A. May; 84(10):3521-5.
30. Kishima H, Poyot T, Bloch J, Dauguet J, Condé F, Dollé F, Hinnen F, Pralong W, Palfi S, Déglon N, et al (2004). Encapsulated GDNF-producing C2C12 cells for Parkinson's disease: a pre-clinical study in chronic MPTP-treated baboons. Neurobiol Dis. Jul;16(2):428-39.
31. Kolde R (2018). pheatmap: Pretty Heatmaps. R package version 1.0.12, https://github.com/raivokolde/pheatmap. (2024 年 11 月 19 日参照)
32. Korotkevich, G., Sukhov, V., Budin, N., Atryomov, M. N (2021). & Sergushichev, A. Fast gene set enrichment analysis. bioRxiv, 1–29.
33. Liberzon A, Birger C, Thorvaldsdóttir H, Ghandi M, Mesirov JP, Tamayo P (2015). The Molecular Signatures Database (MSigDB) hallmark gene set collection. Cell Syst. Dec 23;1(6):417-425.

34. Lopalco A, Cutrignelli A, Denora N, Lopedota A, Franco M, Laquintana V (2018). Transferrin Functionalized Liposomes Loading Dopamine HCl: Development and Permeability Studies across an In Vitro Model of Human Blood-Brain Barrier. Nanomaterials (Basel). Mar 20;8(3):178.
35. Liu Y, Liu J, Chen S, Lei T, Kim Y, Niu S, Wang H, Wang X, Foudeh AM, Tok JB, et al (2019). Soft and elastic hydrogel-based microelectronics for localized low-voltage neuromodulation. Nat Biomed Eng. Jan;3(1):58-68.
36. Li L, Zhang Y, Lu H, Wang Y, Xu J, Zhu J, Zhang C, Liu T (2020). Cryopolymerization enables anisotropic polyaniline hybrid hydrogels with superelasticity and highly deformation-tolerant electrochemical energy storage. Nat Commun. Jan 7;11(1):62.
37. Mahajani S, Raina A, Fokken C, Kügler S, Bähr M (2019). Homogenous generation of dopaminergic neurons from multiple hiPSC lines by transient expression of transcription factors. Cell Death Dis. Nov 27;10(12):898.
38. Martin Frauenlob, Daniel R, King (2019). Modulation and Characterization of the Double Network Hydrogel Surface-Bulk Transition. Macromolecules, 52, 6704−6713.
39. Mo F, Li Q, Liang G, Zhao YW, Wang DH, Huang Y, Wei J, Zhi CY (2021). A self-healing crease-free supramolecular all-polymer supercapacitor. Adv. Sci. 8, 2100072.
40. Martin WRW, Miles M, Zhong Q, Hartlein J, Racette BA, Norris SA, Ushe M, Maiti B, Criswell S, Davis AA, et al (2021). Is Levodopa Response a Valid Indicator of Parkinson's Disease? Mov Disord. Apr;36(4):948-954.
41. Mu Q, Cui K, Wang ZJ, Matsuda T, Cui K, Kato H, Namiki S, Yamazaki T, Frauenlob M, Nonoyama T, et al (2022). Force-triggered rapid microstructure growth on hydrogel surface for on-demand functions, Nat Commun, 13(1):6213.
42. Ng YH, Chanda S, Janas JA, Yang N, Kokubu Y, Südhof TC, Wernig M (2021). Efficient generation of dopaminergic induced neuronal cells with midbrain characteristics. Stem Cell Reports. Jul 13;16(7):1763-1776.
43. Onoa B, Li H, Gagnon-Bartsch JA, Elias LA, Edwards RH. (2010) Vesicular monoamine and glutamate transporters select distinct synaptic vesicle recycling pathways. J Neurosci 30:7917–7927.
44. Park J, Kim SY, Cha GH, Lee SB, Kim S, Chung J (2005). Drosophila DJ-1 mutants show oxidative stress-sensitive locomotive dysfunction. Gene. Nov 21; 361:133-9.

45. Park J, Jeon J, Kim B, Lee MS, Park S, Lim J, Yi J, Lee H, Yang HS, Lee JY (2020). Electrically conductive hydrogel nerve guidance conduits for peripheral nerve regeneration. Adv. Funct. Mater. 30, 2003759.
46. Pardon G, Vander Roest, A.S, Chirikian O, Birnbaum F, Lewis H, Castillo EA, Wilson R, Denisin AK, Blair CA, et al (2024). Tracking single hiPSC-derived cardiomyocyte contractile function using CONTRAX an efficient pipeline for traction force measurement. Nat Commun 15, 5427.
47. R Core Team (2023). _R: A Language and Environment for Statistical Computing_. R Foundation for Statistical Computing, Vienna, Austria, https://www.R-project.org/. (2024 年 11 月 19 日参照)
48. Schneider JS, Rothblat DS (1991). Neurochemical evaluation of the striatum in symptomatic and recovered MPTP-treated cats. Neuroscience. 44(2):421-9.
49. Shannon P, Markiel A, Ozier O, Baliga NS, Wang JT, Ramage D, Amin N, Schwikowski B, Ideker T (2003). Cytoscape: a software environment for integrated models of biomolecular interaction networks. Genome Res. Nov;13(11):2498-504.
50. Subramanian A, Tamayo P, Mootha VK, Mukherjee S, Ebert BL, Gillette MA, Paulovich A, Pomeroy SL, Golub TR, Lander ES, et al (2005). Gene set enrichment analysis: a knowledge-based approach for interpreting genome-wide expression profiles. Proc Natl Acad Sci U S A. Oct 25;102(43):15545-50.
51. Saiki H, Hayashi T, Takahashi R, Takahashi J (2010). Objective and quantitative evaluation of motor function in a monkey model of Parkinson's disease. J Neurosci Methods. Jul 15;190(2):198-204.
52. Supek F, Bošnjak M, Škunca N, Šmuc T (2011). REVIGO summarizes and visualizes long lists of gene ontology terms. PLoS One. 6(7): e21800.
53. Sallouh M, Jarocki M, Sallouh O, Degen P, Faissner A, Weberskirch R (2017). The Synergistic Effect of Cationic Moieties and GRGDSF-Peptides in Hydrogels on Neural Stem Cell Behavior. Macromol Biosci. Mar;17(3).
54. Stamm N, Glotzbach K, Faissner A, Weberskirch R (2022). Concentration Dependent Effect of Quaternary Amines on the Adhesion of U251-MG Cells. Gels. Dec 15;8(12):827.
55. Sheta R, Teixeira M, Idi W, Pierre M, de Rus Jacquet A, Emond V, Zorca CE, Vanderperre B, Durcan TM, Fon EA, et al (2022). Combining NGN2 programming and dopaminergic patterning for a rapid and efficient generation of hiPSC-derived midbrain neurons. Sci Rep. Oct 13;12(1):17176.

56. Suzuka J, Tsuda M, Wang L, Kohsaka S, Kishida K, Semba S, Sugino H, Aburatani S, Mu Q, Cui K, et al (2022). Force-triggered rapid microstructure growth on hydrogel surface for on-demand functions. Nat Commun. Oct 20;13(1):6213.
57. Schloerke B, Cook D, Larmarange J, Briatte F, Marbach M, Thoen E, Elberg A, Huang, D.W., Sherman, B.T., et al (2022). DAVID: a web server for functional annotation and functional clustering of gene lists. Nucleic Acids Research, Volume 50, Issue W1, Pages W216–W221.
58. Tanikawa S, Ebisu Y, Sedlačík T, Semba S, Nonoyama T, Kurokawa T, Hirota A, Takahashi T, Yamaguchi K, Imajo M, et al (2023). Engineering of an electrically charged hydrogel implanted into a traumatic brain injury model for stepwise neuronal tissue reconstruction. Sci Rep. Feb 14;13(1):2233.
59. Tennekes M (2023). _treemap: Treemap Visualization_. R package version 2.4-4, https://CRAN.R-project.org/package=treemap. (2024 年 11 月 19 日参照)
60. Wickham H (2016). ggplot2: Elegant Graphics for Data Analysis. Springer-Verlag New York. ISBN 978-3-319-24277-4.
61. Wang Y, Chen F, Liu Z, Tang Z, Yang Q, Zhao Y, Du S, Chen Q, Zhi C (2019). A Highly Elastic and Reversibly Stretchable All-Polymer Supercapacitor. Angew Chem Int Ed Engl. Oct 28;58(44):15707-15711.
62. Xi J, Liu Y, Liu H, Chen H, Emborg ME, Zhang SC (2012). Specification of midbrain dopamine neurons from primate pluripotent stem cells. Stem Cells. Aug;30(8):1655-63.
63. Xue Y, Zhan X, Sun S, Karuppagounder SS, Xia S, Dawson VL, Dawson TM, Laterra J, Zhang J, Ying M (2019). Synthetic mRNAs Drive Highly Efficient iPS Cell Differentiation to Dopaminergic Neurons. Stem Cells Transl Med. Feb;8(2):112-123.
64. Xu F, Jin H, Wu H, Jiang A, Qiu B, Liu L, Gao Q, Lin B, Kong W, Chen S, et al (2024). Digital light processing printed hydrogel scaffolds with adjustable modulus. Sci Rep. Jul 8;14(1):15695.
65. Xu X, Wang W, Liu Y, Bäckemo J, Heuchel M, Wang W, Nie Y, Iqbal I, Kratz K, Lendlein A, et al (2024). Substrates mimicking the blastocyst geometry revert pluripotent stem cell to naivety. Nat. Mater. https://doi.org/10.1038/s41563-024-01971-4.

66. Yokoyama H, Uchida H, Kuroiwa H, Kasahara J, Araki T (2011). Role of glial cells in neurotoxin-induced animal models of Parkinson's disease. Neurol Sci. Feb;32(1):1-7.
67. Yokoyama H, Kuroiwa H, Kasahara J, Araki T (2011). Neuropharmacological approach against MPTP (1-methyl-4-phenyl-1,2,3,6- tetrahydropyridine)-induced mouse model of Parkinson's disease. Acta Neurobiol Exp (Wars). 71(2):269-80.
68. Yuk H, Lu B, Lin S, Qu K, Xu J, Luo J, Zhao X (2020). 3D printing of conducting polymers. Nat Commun. Mar 30;11(1):1604.
69. Yejin Jo, Lee Y, Heo JH, Son Y, Kim TY, Park K, Kim S, Kim SJ, Jin Y, Park S& Seo J (2024). Universal hydrogel adhesives with robust chain entanglement for bridging soft electronic materials. npj Flexible Electronics volume 8: 39.
70. Zhou X, Zhao F, Guo Y, Rosenberger B, Yu G (2019). Architecting highly hydratable polymer networks to tune the water state for solar water purification. Sci Adv. Jun 28;5(6): 5484.
71. Zhu J, He Y, Wang Y, Cai LH (2024). Voxelated bioprinting of modular double-network bio-ink droplets. Nat Commun. Jul 13;15(1):5902.